

Supporting Information

Boron(III) β -Diketonate-Based Small Molecules for Functional Non-Fullerene Polymer Solar Cells and Organic Resistive Memory Devices

Panpan Li,^a Quanbin Liang,^b Eugene Yau-Hin Hong,^a Chin-Yiu Chan,^a Yat-Hin Cheng,^a Ming-Yi Leung,^a Mei-Yee Chan,^a Kam-Hung Low,^a Hongbin Wu^b and Vivian Wing-Wah Yam^{a*}

^a Institute of Molecular Functional Materials and Department of Chemistry, The University of Hong Kong, Pokfulam Road, Hong Kong, P. R. China

^b Institute of Polymer Optoelectronic Materials and Devices, State Key Laboratory of Luminescent Materials and Devices, South China University of Technology, Guangzhou 510640, P. R. China

*E-mail: wwyam@hku.hk

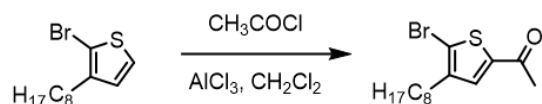
Table of Contents

Synthesis and Characterization	S3
X-Ray Crystal Structure Study	S10
Thermogravimetric Analysis	S14
Differential Scanning Calorimetry	S15
Optical Properties	S16
Electrochemical Studies	S17
Devices Fabrication and Characterization	S19
Computational Details and Studies	S34
NMR and HR-ESI Mass Spectra of Target Compounds	S55
References	S63

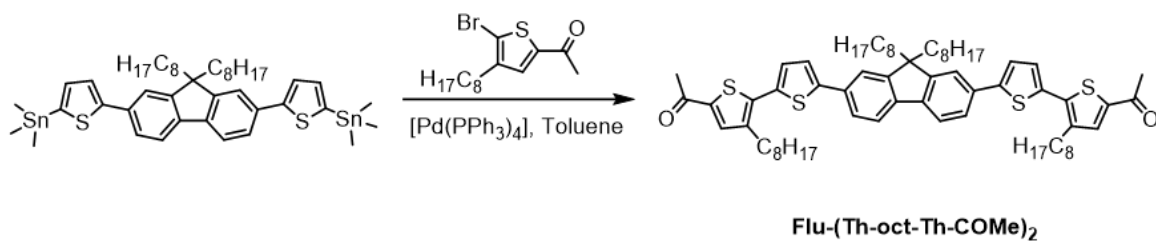
Synthesis and Characterization

Materials and Reagents. ((9,9-Dioctyl-9*H*-fluorene-2,7-diyl)bis(thiophene-5,2-diyl))bis(trimethylstannane)¹ and (4,4,9,9-tetrakis(4-hexylphenyl)-4,9-dihydro-*s*-indaceno[1,2-*b*:5,6-*b'*]dithiophene-2,7-diyl)bis(trimethylstannane)² were synthesized according to the literature reported procedures. All commercially available reagents were of analytical grade and were used as received. All solvents were purified by the Innovative Technology, Inc. PureSolv MD 5 Solvent Purification System before use. Tetra-*n*-butylammonium hexafluorophosphate (Aldrich, 98%, ⁿBu₄NPF₆) was recrystallized at least three times from absolute ethanol before use.

Characterization and Instrumentation. ¹H NMR and ¹⁹F{¹H} NMR spectroscopy were performed using a Bruker AV400 NMR spectrometer at 298 K with chemical shifts (δ , ppm) relative to tetramethylsilane (Me₄Si) for the ¹H NMR and trichlorofluoromethane (CFCl₃) for the ¹⁹F{¹H} NMR spectra. ¹¹B{¹H} NMR spectra were recorded on a Bruker DRX 500 NMR spectrometer at 298 K with chemical shifts (δ , ppm) reported relative to BF₃•OEt₂. High resolution electrospray ionization (ESI) and high resolution electron ionization (EI) mass spectroscopy were recorded on a Bruker MaXis II Ultrahigh-Resolution Time-of-Flight Mass Spectrometer and a Thermo Scientific DFS High Resolution Magnetic Sector Mass Spectrometer, respectively. Elemental analyses (C, H and N) were carried out at the Institute of Chemistry, Chinese Academy of Sciences, Beijing, People's Republic of China, using a Carlo Erba 1106 elemental analyzer.

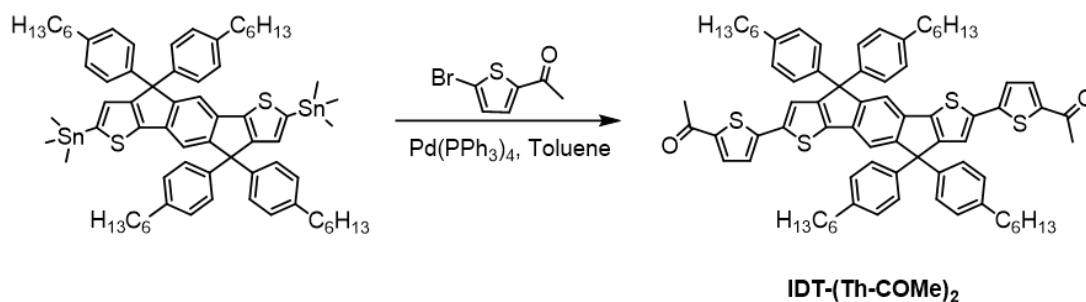


1-(5-Bromo-4-octylthiophen-2-yl)ethan-1-one. To a stirred solution of aluminum chloride (293 mg, 2.2 mmol) in anhydrous dichloromethane (15 mL) at 0 °C was added acetyl chloride (0.16 mL, 2.2 mmol). After stirring at 0 °C for 20 min, a solution of 2-bromo-3-octylthiophene (550 mg, 2.0 mmol) in dichloromethane (10 mL) was added dropwise to the reaction mixture. The resulting solution was then gradually warmed up to room temperature and stirred for another 1.5 hours. The reaction was quenched by the addition of deionized water and extracted with dichloromethane. The combined organic layer was dried over anhydrous magnesium sulfate, filtered and the filtrate was evaporated to dryness under reduced pressure. The crude product was purified by flash column chromatography on a silica gel using hexane–dichloromethane (2:1, v/v) as eluent to afford, after solvent removal, a pale yellow oil. Yield: 495 mg (78%). ¹H NMR (500 MHz, CDCl₃, 298 K, relative to Me₄Si, δ /ppm): δ 0.88 (t, J = 7.5 Hz, 3H, –CH₃), 1.27–1.32 (m, 10H, –CH₂–), 1.56–1.62 (m, 2H, –CH₂–), 2.49 (s, 3H, –OCH₃), 2.56 (t, 2H, J = 7.5 Hz, –CH₂–), 7.36 (s, 1H, thienyl). HRMS (positive EI) calcd for C₁₄H₂₁BrOS: m/z = 316.0496 [M]⁺; found: 316.0479 [M]⁺.



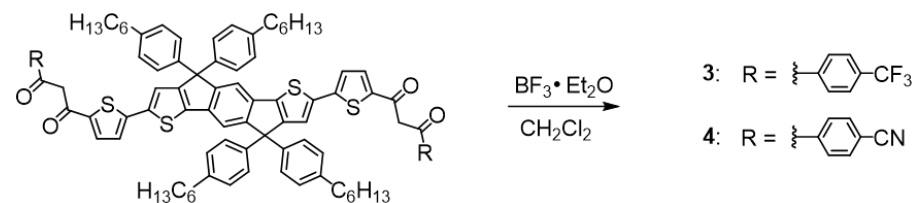
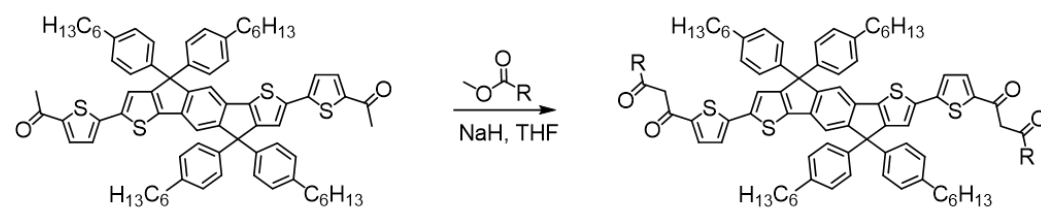
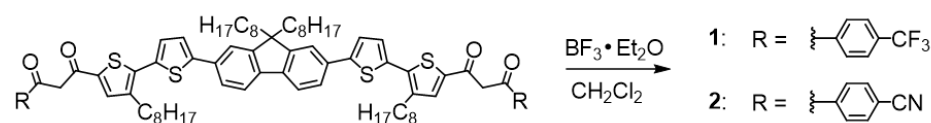
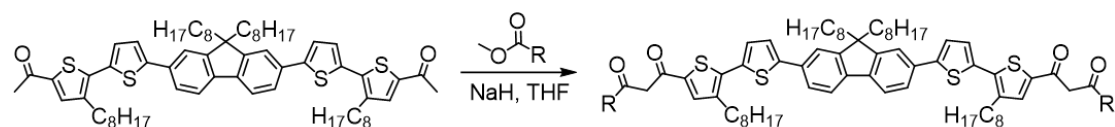
1,1'-((9,9-Dioctyl-9H-fluorene-2,7-diyl)bis(3-octyl-[2,2'-bithiophene]-5',5-diyl))-bis(ethan-1-one) (Flu-(Th-oct-Th-COMe)₂. To a stirred solution mixture of ((9,9-dioctyl-9H-fluorene-2,7-diyl)bis(thiophene-5,2-diyl))bis(trimethylstannane) (700 mg, 0.80 mmol) and 1-(5-bromo-4-octylthiophen-2-yl)ethan-1-one (630 mg, 2.0 mmol) in anhydrous toluene (40 mL) was added tetrakis(triphenylphosphine)palladium(0) (90 mg, 10 mol%). The reaction mixture was heated to reflux overnight. After cooling to room temperature, the reaction mixture was quenched by the addition of deionized

water and extracted with dichloromethane. The combined organic layer was dried over anhydrous magnesium sulfate, filtered and the filtrate was evaporated to dryness under reduced pressure. The crude product was then purified by column chromatography on silica gel using hexane–dichloromethane (1:1, v/v) as eluent to give, after solvent removal, an orange solid. Yield: 680 mg (83%). ¹H NMR (400 MHz, CDCl₃, 298 K, relative to relative to Me₄Si, δ/ppm): δ 0.67–0.75 (m, 4H, –CH₂–), 0.78 (t, *J* = 6.8 Hz, 6H, –CH₃), 0.88 (t, *J* = 6.8 Hz, 6H, –CH₃), 1.07–1.16 (m, 20H, –CH₂–), 1.29–1.43 (m, 20H, –CH₂–), 1.69–1.71 (m, 4H, –CH₂–), 2.01–2.04 (m, 4H, –CH₂–), 2.55 (s, 6H, –(CO)CH₃), 2.84 (t, *J* = 6.8 Hz, 4H, –CH₂–), 7.25 (d, *J* = 3.8 Hz, 2H, thienyl), 7.37 (d, *J* = 3.8 Hz, 2H, thienyl), 7.54 (s, 2H, thienyl), 7.56 (d, *J* = 1.6 Hz, 2H, phenyl of fluorene), 7.61 (dd, *J* = 7.9, 1.6 Hz, 2H, phenyl of fluorene), 7.71 (d, *J* = 7.9 Hz, 2H, phenyl of fluorene). HRMS (positive ESI) calcd for C₆₅H₈₇O₂S₄: *m/z* = 1027.5589 [M+H]⁺; found: 1027.5583 [M+H]⁺.



1,1'-((4,4,9,9-Tetrakis(4-hexylphenyl)-4,9-dihydro-*s*-indaceno[1,2-*b*:5,6-*b'*]dithiophene-2,7-diyl)bis(thiophene-5,2-diyl))bis(ethan-1-one) (IDT-(Th-COMe)₂). The procedure was similar to that used to prepare **Flu-(Th-oct-Th-COMe)₂**, except (4,4,9,9-tetrakis(4-hexylphenyl)-4,9-dihydro-*s*-indaceno[1,2-*b*:5,6-*b'*]dithiophene-2,7-diyl)bis(trimethylstannane) (986 mg, 0.8 mmol) and 1-(5-bromothiophen-2-yl)ethan-1-one (410 mg, 2 mmol) were used in place of ((9,9-dioctyl-9*H*-fluorene-2,7-diyl)bis(thiophene-5,2-diyl))bis(trimethylstannane) and 1-(5-bromo-4-octylthiophen-2-yl)ethan-1-one, respectively. The product was isolated as an orange solid. Yield: (638 mg, 69%). ¹H NMR (400 MHz, CDCl₃, 298 K, relative to relative to Me₄Si, δ/ppm): δ 0.87 (t, *J* = 6.7 Hz, 12H, –CH₃), 1.28–1.33 (m, 24H, –CH₃), 1.56–1.58 (m, 8H, –CH₂–),

2.53 (s, 6H, $-(CO)CH_3$), 2.54–2.58 (m, 8H, $-CH_2-$), 7.08 (d, $J = 8.3$ Hz, 8H, phenyl), 7.13 (d, $J = 4.0$ Hz, 2H, thienyl), 7.16 (d, $J = 8.3$ Hz, 8H, phenyl), 7.22 (s, 2H, thienyl), 7.41 (s, 2H, phenyl), 7.55 (d, $J = 4.0$ Hz, 2H, thienyl). HRMS (positive ESI) calcd for $C_{76}H_{82}O_2S_4$: $m/z = 1155.7276$ $[M+H]^+$; found: 1155.5270 $[M+H]^+$.



General synthetic procedures for β -diketonates and their corresponding boron(III)

β -diketonates 1–4. To a stirred solution of **Flu-(Th-oct-Th-COMe)₂** (1.03 g, 1 mmol) or **IDT-(Th-COMe)₂** (1.15 g, 1 mmol) in anhydrous tetrahydrofuran (5 mL) at 0 °C was added sodium hydride (60% dispersion in mineral oil, 120 mg, 3 mmol). The resulting mixture was stirred at 0 °C for 15 min and the corresponding methyl 4-(trifluoromethyl)benzoate (0.20 g, 1 mmol) or methyl 4-cyanobenzoate (0.16 g, 1 mmol) was subsequently added dropwise. After gradually warming up to room temperature, the reaction mixture was heated to reflux overnight. The reaction mixture was quenched by the addition of an aqueous HCl solution (1 M) and extracted with dichloromethane. The combined organic layer was dried over anhydrous magnesium sulfate, filtered and

the filtrate was evaporated to dryness under reduced pressure. The obtained crude β -diketonate was used directly for the next step without further purification. To a stirred solution of the β -diketonate (0.50 mmol) in anhydrous dichloromethane (45 mL) was added boron trifluoride diethyl etherate ($\geq 46\%$ BF₃ basis, 0.20 mL, 0.76 mmol). The reaction mixture was heated to reflux overnight. The reaction was quenched by the addition of deionized water and extracted with dichloromethane. The combined organic layer was dried over anhydrous magnesium sulfate, filtered and the filtrate was evaporated to dryness under reduced pressure. The crude product was then purified by flash column chromatography on silica gel using hexane–dichloromethane (1:1, v/v) as eluent to give the product, after solvent removal, as a dark red solid.

1. Yield: 309 mg (37%). ¹H NMR (400 MHz, CDCl₃, 298 K, relative to Me₄Si, δ /ppm): δ 0.63–0.70 (m, 4H, –CH₂–), 0.79 (t, J = 6.8 Hz, 6H, –CH₃), 0.89 (t, J = 6.8 Hz, 6H, –CH₃), 1.08–1.19 (m, 20H, –CH₂–), 1.34–1.50 (m, 20H, –CH₂–), 1.74–1.81 (m, 4H, –CH₂–), 1.99–2.08 (m, 4H, –CH₂–), 2.90–2.94 (m, 4H, –CH₂–), 6.93 (s, 2H, –C(O)–CHC(O)–), 7.41 (d, J = 4.0 Hz, 2H, thienyl), 7.45 (d, J = 4.0 Hz, 2H, thienyl), 7.60 (s, 2H, phenyl of fluorene), 7.65 (d, J = 7.9 Hz, 2H, phenyl of fluorene), 7.74 (d, J = 7.9 Hz, 2H, phenyl of fluorene), 7.80 (d, J = 8.4 Hz, 4H, phenyl), 8.00 (s, 2H, thienyl), 8.21 (d, J = 8.4 Hz, 4H, phenyl). ¹⁹F{¹H}NMR (376.4 MHz, CDCl₃, 298 K, relative to CFCl₃, δ /ppm): δ –63.17 (d, J_{F-F} = 26.3 Hz, 6F, –CF₃), –140.49 (d, J_{F-F} = 26.3 Hz, 4F, –BF₂, 4:1 ratio due to the natural abundance distribution of B isotopes). ¹¹B{¹H} NMR (160.5 MHz, CDCl₃, 298 K, relative to BF₃•OEt₂, δ /ppm): δ 1.09. HRMS (positive ESI) calcd for C₈₁H₉₀B₂F₁₀O₄S₄: m/z = 1466.5748 [M]⁺; found: 1467.5766 [M]⁺. Elemental analyses: Found (%): C, 66.29; H, 6.18. Calcd for C₈₁H₉₀B₂F₁₀O₄S₄: C, 66.30; H, 6.18.

2. Yield: 0.62 g (45%). ¹H NMR (400 MHz, CDCl₃, 298 K, relative to Me₄Si, δ /ppm): δ 0.65–0.75 (m, 4H, –CH₂–), 0.78 (t, J = 6.8 Hz, 6H, –CH₃), 0.88 (t, J = 6.8 Hz, 6H, –CH₃), 1.07–1.18 (m, 20H, –CH₂–), 1.25–1.49 (m, 20H, –CH₂–), 1.74–1.78 (m, 4H, –CH₂–), 2.03–2.07 (m, 4H, –CH₂–), 2.89–2.93 (m, 4H, –CH₂–), 6.90 (s, 2H,

–C(O)–CHC(O)–), 7.42 (d, $J = 3.9$ Hz, 2H, thienyl), 7.45 (d, $J = 3.9$ Hz, 2H, thienyl), 7.59 (s, 2H, phenyl of fluorene), 7.64 (d, $J = 7.9$ Hz, 2H, phenyl of fluorene), 7.74 (d, $J = 7.9$ Hz, 2H, phenyl of fluorene), 7.82 (d, $J = 8.5$ Hz, 4H, phenyl), 8.00 (s, 2H, thienyl), 8.18 (d, $J = 8.5$ Hz, 4H, phenyl). $^{19}\text{F}\{^1\text{H}\}$ NMR (376.4 MHz, CDCl_3 , 298 K, relative to CFCl_3 , δ/ppm): δ –140.42 (d, $J_{\text{F-F}} = 22.6$ Hz, $-\text{BF}_2$, 4:1 ratio due to the natural abundance distribution of B isotopes). $^{11}\text{B}\{^1\text{H}\}$ NMR (160.5 MHz, CDCl_3 , 298 K, relative to $\text{BF}_3\cdot\text{OEt}_2$, δ/ppm): δ 1.05. HRMS (positive ESI) calcd for $\text{C}_{83}\text{H}_{92}\text{B}_2\text{F}_4\text{N}_2\text{O}_8\text{S}_4$: $m/z = 735.2930$ $[\text{M}+2\text{HCOOH}-2\text{H}]^{2+}$; found: 735.2936 $[\text{M}+2\text{HCOOH}-2\text{H}]^{2+}$. Elemental analyses: Found (%): C, 70.65; H, 6.68; N, 2.26. Calcd for $\text{C}_{81}\text{H}_{90}\text{B}_2\text{F}_4\text{N}_2\text{O}_4\text{S}_4$: C, 70.42; H, 6.57; N, 2.03.

3. Yield: 0.94 g (56%). ^1H NMR (400 MHz, CDCl_3 , 298 K, relative to Me_3Si , δ/ppm): δ 0.87 (t, $J = 6.7$ Hz, 12H, $-\text{CH}_3$), 1.28–1.34 (m, 24H, $-\text{CH}_3$), 1.56–1.60 (m, 8H, $-\text{CH}_2-$), 2.56–2.60 (m, 8H, $-\text{CH}_2-$), 6.91 (s, 2H, $-\text{C}(\text{O})-\text{CHC}(\text{O})-$), 7.11 (d, $J = 8.4$ Hz, 8H, phenyl), 7.17 (d, $J = 8.4$ Hz, 8H, phenyl), 7.31 (d, $J = 4.2$ Hz, 2H, thienyl), 7.37 (s, 2H, thienyl), 7.49 (s, 2H, phenyl), 7.77 (d, $J = 8.4$ Hz, 4H, phenyl), 8.02 (d, $J = 4.2$ Hz, 2H, thienyl), 8.17 (d, $J = 8.4$ Hz, 4H, phenyl). $^{19}\text{F}\{^1\text{H}\}$ NMR (376.4 MHz, CDCl_3 , 298 K, relative to CF_3Cl , δ/ppm): δ –63.16 (d, $J_{\text{F-F}} = 26.3$ Hz, 6F, $-\text{CF}_3$), –140.45 (d, $J_{\text{F-F}} = 26.3$ Hz, 4F, $-\text{BF}_2$, 4:1 ratio due to the natural abundance distribution of B isotopes). $^{11}\text{B}\{^1\text{H}\}$ NMR (160.5 MHz, CDCl_3 , 298 K, relative to $\text{BF}_3\cdot\text{OEt}_2$, δ/ppm): δ 1.03. HRMS (positive ESI) calcd for $\text{C}_{92}\text{H}_{86}\text{B}_2\text{F}_{10}\text{O}_4\text{S}_4\text{Na}$: $m/z = 1617.5333$ $[\text{M}+\text{Na}]^+$; found: 1617.5353 $[\text{M}+\text{Na}]^+$. Elemental analyses: Found (%): C, 69.15; H, 5.36. Calcd for $\text{C}_{92}\text{H}_{86}\text{B}_2\text{F}_{10}\text{O}_4\text{S}_4$: C, 69.26; H, 5.43.

4. Yield: 0.63 (42%). ^1H NMR (400 MHz, CDCl_3 , 298 K, relative to Me_3Si , δ/ppm): δ 0.87 (t, $J = 6.8$ Hz, 12H, $-\text{CH}_3$), 1.25–1.36 (m, 24H, $-\text{CH}_2-$), 1.56–1.63 (m, 8H, $-\text{CH}_2-$), 2.58 (t, $J = 6.8$ Hz, 8H, $-\text{CH}_2-$), 6.89 (s, 2H, $-\text{C}(\text{O})-\text{CHC}(\text{O})-$), 7.11 (d, $J = 8.3$ Hz, 8H, phenyl), 7.17 (d, $J = 8.3$ Hz, 8H, phenyl), 7.32 (d, $J = 4.3$ Hz, 2H, thienyl),

7.38 (s, 2H, thienyl), 7.48 (s, 2H, phenyl), 7.82 (d, $J = 8.4$ Hz, 4H, phenyl), 8.03 (d, $J = 4.3$ Hz, 2H, thienyl), 8.16 (d, $J = 8.4$ Hz, 4H, phenyl). $^{19}\text{F}\{^1\text{H}\}$ NMR (376.4 MHz, CDCl_3 , 298 K, relative to CFCl_3 , δ/ppm): δ -140.36 (d, $J_{\text{F-F}} = 26.3$ Hz, $-\text{BF}_2$, 4:1 ratio due to the natural abundance distribution of B isotopes); $^{11}\text{B}\{^1\text{H}\}$ NMR (160.5 MHz, CDCl_3 , 298 K, relative to $\text{BF}_3 \cdot \text{OEt}_2$, δ/ppm): δ 0.96. HRMS (positive ESI) calcd for $\text{C}_{92}\text{H}_{86}\text{B}_2\text{F}_4\text{N}_2\text{O}_4\text{S}_4$: $m/z = 1508.5593$ $[\text{M}]^+$; found: 1508.5613 $[\text{M}]^+$. Elemental analyses: Found (%): C, 73.44; H, 5.89; N, 1.95. Calcd for $\text{C}_{92}\text{H}_{86}\text{B}_2\text{F}_4\text{N}_2\text{O}_4\text{S}_4$: C, 73.20; H, 5.74; N, 1.86.

X-Ray Crystal Structure Study

X-Ray Crystallography. Single-crystal X-ray data were collected on a Bruker D8 VENTURE MetalJet Photon II CPAD X-Ray Diffractometer, using Ga $K\alpha$, radiation (1.34138 Å). Data collection was done using *APEX3* v2018.7-2 (Bruker-AXS, 2018) program. Cell refinement and data reduction were done using *SAINT* V8.38A (Bruker AXS Inc., 2017) program. The structure was solved using *SHELXT* 2014/5 (Sheldrick, 2014) program and refined by *SHELXL2018/3* (Sheldrick, 2018) program. All e.s.d.'s (except the e.s.d. in the dihedral angle between two least-squares (l.s.) planes) are estimated using the full covariance matrix. Due to the high degree of freedom of the octyl chains, atomic coordinates determination of the octyl chain atoms from electron density map was unsuccessful. Suitable geometrical restraints were applied on the octyl chains to achieve a chemically reasonable model. Yawing disorder of the terminal group of the planar conjugated system was treated as two disordered parts. Chlorobenzene solvent molecules were found to co-crystallize and diffuse in the lattice. The corresponding electron density was treated by PLATON/SQUEEZE procedure and the solvent molecules were omitted in the final model. The X-ray crystallographic data for compound **1** have been deposited at the Cambridge Crystallographic Data Centre (CCDC), under the deposition number CCDC 1960933. The data can be obtained free of charge from the Cambridge Crystallographic Data Center via www.ccdc.cam.ac.uk/data_request/cif.

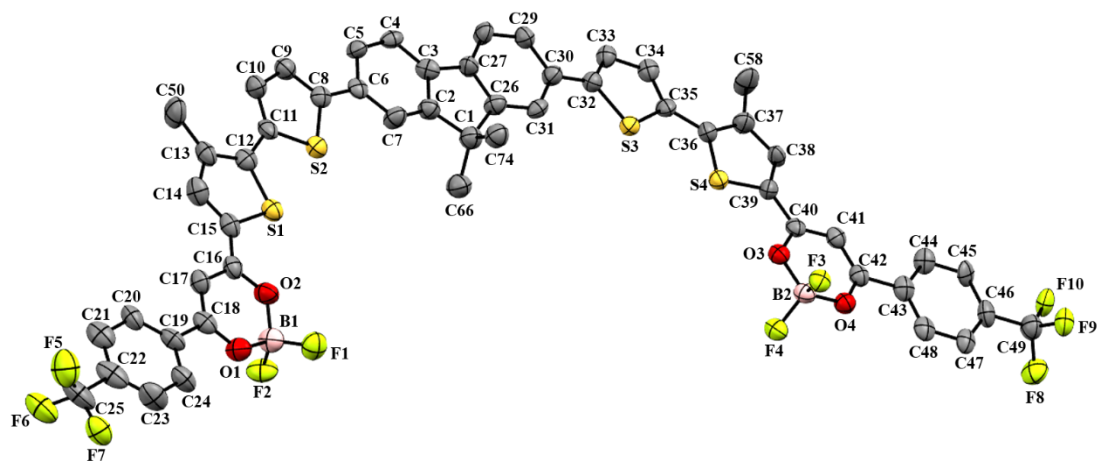


Fig. S1 Perspective view of the molecular structure of **1** with atomic numbering.

Carbon atoms of the octyl chains, except the alpha carbon, are omitted for clarity.

Riding hydrogen atoms and disorder parts have also been omitted. The thermal ellipsoids were shown at the 50% probability level.

Table S1 Selected noncovalent bond contacts, bond distances and torsional angles of compound **1**.

Noncovalent bond contacts / Å			
S1...S2	3.11	S1...O2	2.86
C7-H7...S2	2.72	C23-H23...F7	2.21
C24-H24...O1	2.38	C72...F1	2.67
C17-H17...F2	2.53	C29-H29...F10	2.47
C31-H31...S3	2.74	C47-H47...F6	2.49
C52-H52...S1	2.79	C72-H72...F1	1.93
C78-H78...F1	2.48	C81-H81...O4	2.46

Torsion angle / °			
C7-C6-C8-C9	172.09	C7-C6-C8-S2	8.34
S2-C11-C12-C13	178.11	S2-C11-C12-S1	4.95
S1-C15-C16-C17	178.88	S1-C15-C16-O2	5.93
O1-C18-C19-C20	172.13	O1-C18-C19-C24	7.62

Table S2 Crystal structure determination data of **1**.

Compound	1
Empirical formula	C ₈₁ H ₉₀ B ₂ F ₁₀ O ₄ S ₄ , C ₆ H ₅ Cl
Formula weight	1579.93
Temperature, K	103
Wavelength, Å	1.34138
Crystal system	Tetragonal
Space group	$\bar{1}42d$
<i>a</i> , Å	48.916(3)
<i>b</i> , Å	48.916(3)
<i>c</i> , Å	13.7593(10)
α , deg	90.00(0)
β , deg	114.68(3)
γ , deg	90.00(0)
Volume, Å ³	32923(4)
<i>Z</i>	16
Density (Calcd), g cm ⁻³	1.275
<i>F</i> ₀₀₀	13280
Crystal size, mm	0.10× 0.07 0.04
θ range for data collection, deg	2.5 to 53.0
Index ranges	$-45 \leq h \leq 58$ $-58 \leq k \leq 58$ $-16 \leq l \leq 15$
Reflections collected (unique)	8009
Goodness-of-fit on <i>F</i> ²	1.13
Final R indices [<i>I</i> > 2σ(<i>I</i>)]	<i>R</i> ₁ = 0.098, <i>wR</i> ₂ = 0.324
Largest diff. peak and hole, e Å ⁻³	-0.54 and 0.79

Thermogravimetric Analysis

Thermal analyses were performed on a TA instruments Q50 thermogravimetric analyzer (TGA) with a heating rate of 10 °C min⁻¹ under nitrogen atmosphere, in which the decomposition temperature (T_d) is defined as the temperature at which the material showed a 5% weight loss.

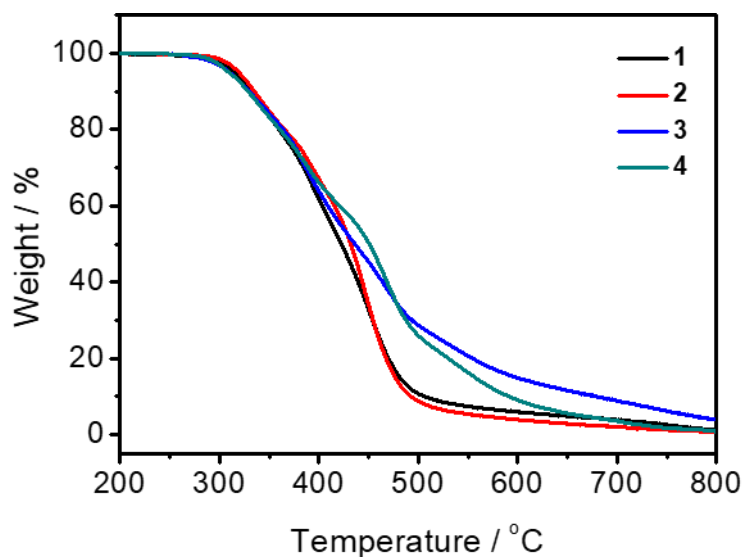


Fig. S2 TGA traces of 1–4.

Table S3 Thermogravimetric analysis data of 1–4.

Compound	$T_d / ^\circ\text{C}^a$
1	315
2	319
3	310
4	309

^a T_d was determined at 5% weight loss.

Differential Scanning Calorimetry

The differential scanning calorimetry (DSC) measurements were performed on a PerkinElmer STA6000 instrument. A sample of 5 to 10 mg was weighed and the heating cycle was conducted from room temperature to 230 °C with a heating/cooling rate of 10 °C min⁻¹ under a nitrogen atmosphere.

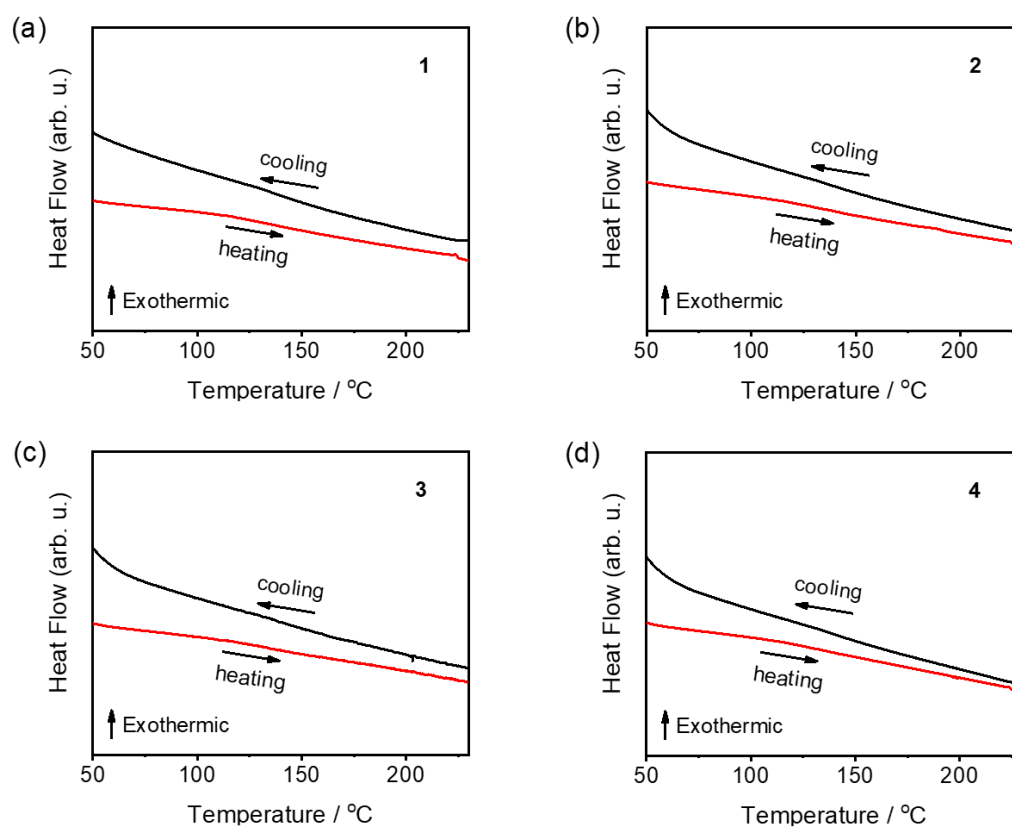


Fig. S3 DSC curves of 1–4 with a heating/cooling rate of 10 °C min⁻¹.

Optical Properties

The UV–vis absorption spectra were recorded on a Varian Cary 50 spectrophotometer equipped with a Xenon flash lamp.

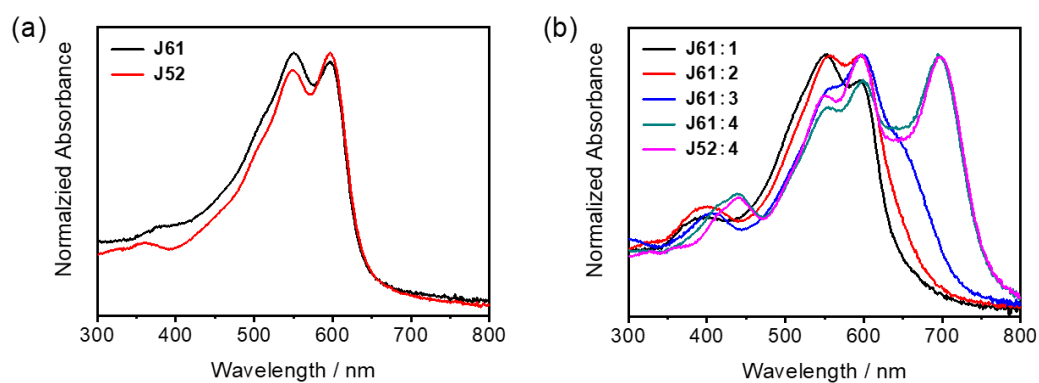


Fig. S4 (a) Normalized absorption spectra of the thermally annealed pristine **J61**, **J52** thin films and (b) **J61:1–4**, **J52:4** blend films spin-coated from chlorobenzene solution.

Electrochemical Studies

Cyclic voltammetric (CV) measurements were performed by using a CH Instruments, Inc. model CHI 620A electrochemical analyzer. Electrochemical measurements were performed in dichloromethane solutions with 0.1 mol dm^{-3} $n\text{Bu}_4\text{NPF}_6$ as supporting electrolyte at room temperature. A three-electrode system was employed, with a Ag/AgNO₃ (0.1 mol dm^{-3} in acetonitrile), a glassy carbon (CH Instrument, Inc.) and a platinum wire as the reference electrode, the working electrode and the counter electrode, respectively, in a glass cell with compartments separating the working electrode and the reference electrode from the counter electrode. The ferrocenium/ferrocene couple (Fc^+/Fc) was used as the internal reference. All solutions for electrochemical studies were deaerated with prepurified argon gas prior to measurements.

With the same electron-donating core, the potentials for the first oxidation are found to be similar, that is, *ca.* +1.13 V vs. saturated calomel electrode (SCE) for **1** and **2**, and *ca.* +1.23 V vs. SCE for **3** and **4**, respectively. The less positive potentials of **3** and **4** than those of **1** and **2** can be explained by the more electron-donating nature of the indacenodithiophene (IDT) core in both **3** and **4**, which would destabilize the HOMO level. On the other hand, the less negative reduction potentials of **2** (−0.66 V vs. SCE) and **4** (−0.62 V vs. SCE) in comparison to those of **1** (−0.69 V vs. SCE) and **3** (−0.67 V vs. SCE) are due to the more electron-deficient nature of the cyano substituent, which would stabilize the LUMO.

Table S4 Electrochemical data of **1–4**.^a

Compound	$E_{1/2}^{\text{ox}} / \text{V vs SCE}^b$ ($\Delta E_p / \text{mV}$)	$E_{1/2}^{\text{red}} / \text{V vs SCE}^b$ ($\Delta E_p / \text{mV}$) [$E_{\text{pc}} / \text{V vs SCE}$] ^c
1	+1.24 (66), +1.37 (60)	-0.69 (58), [-1.49], [-1.67]
2	+1.23 (74), +1.38 (65)	-0.66 (80), -1.42 (75)
3	+1.13 (76), +1.48 (75)	-0.67 (66), [-1.51], [-1.65]
4	+1.13 (71), +1.48 (75)	-0.62 (70), -1.38 (75)

^a 0.1 M ⁿBu₄NPF₆ as supporting electrolyte at room temperature; scan rate 100 mV s⁻¹;

$E^{\circ}(\text{Fc}^+/\text{Fc}) = +0.46 \text{ V vs SCE}$ in dichloromethane. ^b $E_{1/2} = (E_{\text{pa}} + E_{\text{pc}})/2$; E_{pc} is peak anodic potential; E_{pa} and E_{pc} are peak anodic and peak cathodic potentials, respectively.

^c Irreversible reduction wave.

Device Fabrication and Characterization

OSC Device Fabrication and Characterization. Inverted OSC devices with the structure of indium tin oxide (ITO)/ZnO (40 nm)/active layer (1:1, w/w; 100±10 nm)/MoO₃ (7.5 nm)/Al (80 nm) were fabricated, in which ITO/ZnO, and MoO₃/Al were used as the cathode and the anode, respectively. Copolymers **J52** and **J61** were applied as donor materials. OSC devices were fabricated on patterned ITO-coated glass substrates. The substrates were cleaned with Decon 90, rinsed with deionized water, dried in an oven, and treated in a UV ozone chamber. A 40 nm-thin layer of ZnO was spin-coated onto the ITO surface. After being baked at 150 °C for 20 minutes, the substrates were transferred into a nitrogen-filled glove box. A chlorobenzene solution of donor (**J61** or **J52**):acceptor (**1–4**) blend (1:1, w/w, 20 mg mL⁻¹) was spin-coated at 1100 rpm for 30 seconds onto the substrate. The substrate was then subjected to thermal annealing at 110 °C for 10 minutes before thermal deposition of MoO₃ and Al at a rate of 0.1–0.2 nm s⁻¹ without vacuum break. For comparison, thermal deposition of MoO₃ and Al was also performed on the as-casted **J52:4** substrate. A shadow mask was used to define the cathode and to make four 0.16 cm² devices on each substrate. All devices were encapsulated before measurements. The active layer thickness was measured using a Dektak 150 profilometer. The current density–voltage (*J–V*) characteristics were recorded using a Keithley 2400 source meter under an AM1.5G solar simulator (Oriel model 91192). Incident photo-to-current efficiency (IPCE) spectra were recorded using a solar cell–photodetector responsivity measurement system (Enlitech Inc.) calibrated with a certified mono-crystal silicon reference cell.

Transient Photovoltage (TPV) and Photocurrent (TPC) measurements. TPV and TPC measurements were carried out by a well-established experimental setup.³ Charge carriers were generated by a laser pulse excitation at 532 nm, with a pulse width of 8 ns at a frequency of 20 Hz from an Nd:YAG solid-state nanosecond pulse laser (Q-smart 100 of Quantel). For TPV measurement, the signal was recorded on a Tektronix

DPO4014 oscilloscope with 1 M Ω input impedance under open-circuit condition. The V_{oc} of the devices was tuned by adjusting the illumination intensity of a 100 W bromine tungsten lamp through the use of neutral density filters, producing steady-state illumination intensity between 0.1 and 100 mW cm⁻² (corresponding to 0.001–1.0 sun). The power of the pulsed laser was attenuated by a set of neutral density filters so that the amplitude of TPV(ΔV) is much smaller (< 5%) when compared to the V_{oc} of that under standard 1 sun illumination. With these conditions, the TPV data can be described by a mono-exponential decay curve, following $\Delta V = V_p \exp(-t/\Delta\tau)$. Thus, the perturbation carrier decay lifetime ($\Delta\tau$) can be determined via an exponential fit with the total charge density (n) and their lifetime in a device at open voltage under varied light intensity deduced. For the TPC measurement, the signal was collected by recording the transient photovoltage across a 50 Ω load resistor through the use of a Tektronix DPO4014 oscilloscope. The transient photovoltage in TPC measurement was generated at the same pulse intensity as TPV measurement, and was converted to current according to the Ohm's law. All the transient data were obtained by averaging 32 measurements. The TPV measurement was performed at open circuit condition, where all the excess charge carriers were forced to recombine inside the device such that no charge carriers were collected at the electrodes. The TPC measurement was carried out under short circuit conditions, which enabled the collection of most of the free charge carriers.

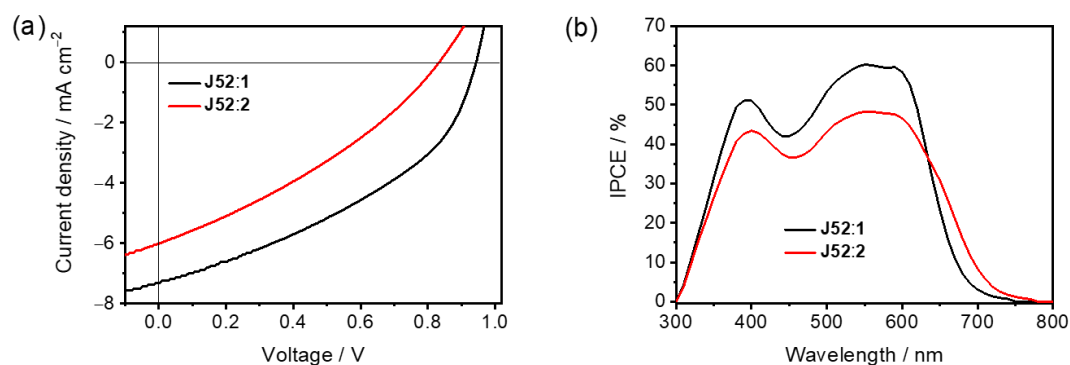


Fig. S5 (a) Representative J - V characteristics and (b) the IPCE spectra of devices using **J52** as the donor material (1:1, w/w; thermal annealing at 110 °C for 10 min, under the illumination of AM1.5G, 100 mW cm⁻²).

Table S5 Photovoltaic parameters of OSC devices using **J52** as the donor material.^a

Active layer	J_{sc} / mA cm ⁻²	V_{oc} / V	FF	PCE / %
J52:1 ^b	7.31 (7.25 ± 0.05)	0.95 (0.95 ± 0.01)	39.85 (39.75 ± 0.10)	2.76 (2.65 ± 0.11)
J52:2 ^b	6.02 (5.98 ± 0.04)	0.83 (0.82 ± 0.01)	32.75 (32.60 ± 0.15)	1.64 (1.52 ± 0.12)
J52:3 ^b	6.86 (6.82 ± 0.03)	0.73 (0.73 ± 0.01)	36.84 (36.75 ± 0.09)	1.84 (1.05 ± 0.09)
J52:4 ^c	6.52 (6.44 ± 0.08)	0.82 (0.81 ± 0.01)	54.20 (54.03 ± 0.17)	2.90 (2.75 ± 0.15)

^a Under the illumination of AM1.5G, 100 mW cm⁻²; average values and deviations in parentheses, calculated from 10 devices. ^b Thermal annealing at 110 °C for 10 min. ^c As-cast films.

Charge Carrier Mobilities Measurements. The hole-only devices with the structure of ITO/poly(3,4-ethylenedioxythiophene) polystyrene sulfonate (PEDOT:PSS)/active layer/MoO₃/Al and the electron-only devices with the structure of ITO/ZnO/active layer/poly [(9,9-bis(3'-(*N,N*-dimethylamino)propyl)-2,7-fluorene)-alt-2,7-(9,9-dioctylfluorene)] (PFN)/Al were fabricated. The charge carrier mobility was determined by fitting the current-bias characteristics in the dark using a field-independent space charge limited current (SCLC) model following the Mott-Gurney law given by $J = \frac{9}{8} \epsilon_0 \epsilon_r \mu \frac{V^2}{L^3}$, where J is the current density, ϵ_0 is the permittivity of free space, ϵ_r is the relative permittivity of the active layer, μ is the carrier mobility, L is the film thickness of the active layer, and V is the effective voltage which is determined by subtracting the built-in voltage (V_{bi}) from the applied voltage ($V_{bi} = V_{appl} - V_{bi}$).

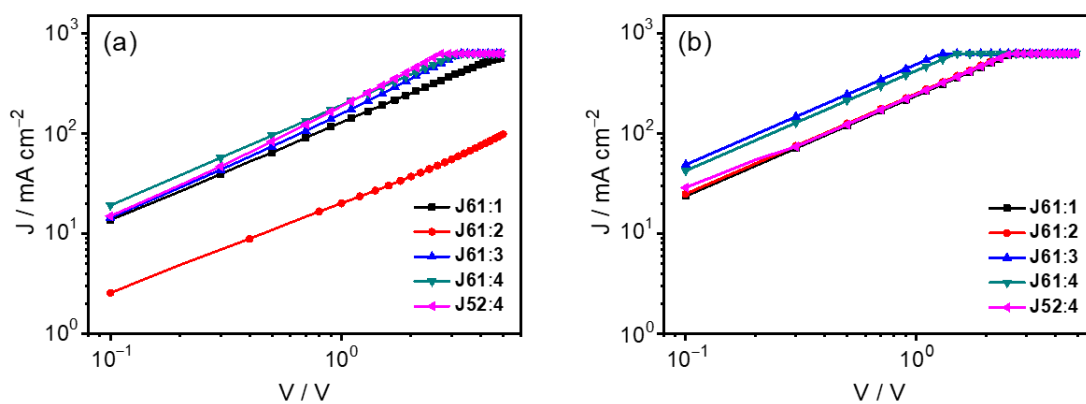


Fig. S6 J - V characteristic curves of (a) hole-only and (b) electron-only devices fabricated with the **J61:1–4** and **J52:4** blends.

Photoluminescence Quenching Studies. The photoluminescence (PL) spectra were recorded using an Edinburgh Instruments FS5 spectrofluorometer equipped with a R928P PMT detector. The PL spectra of the pristine **J61**, **J52** and **1–4** thin films and the **J61:1–4** and **J52:4** blend films under the same thermal annealing condition as the corresponding OSC devices were recorded (Table S6, Fig. S7 and Fig. S8).

Specifically, upon excitation at the absorption maximum of the pristine **J61** thin film at 560 nm, the PL intensity of **J61** is found to be strongly quenched in all the **J61:1–4** blend films (Fig. S7a, c and Fig. S8a, c). This phenomenon indicates that the photogenerated excitons in the **J61** polymeric donor can be dissociated at the interfaces of **J61** and **1–4**, accompanying with efficient electron transfer from **J61** to **1–4**. Meanwhile, by blending **J61** with **1–4**, the PL intensity of **1–4** is also found to be significantly quenched, upon exciting at the corresponding absorption maximum of the respective pristine thin film (Fig. S7b, d and Fig. S8b, d). Likewise, this indicates that excitons generated in the **1–4** acceptor phases can be dissociated at the heterointerfaces of **J61** and **1–4**, verifying an efficient hole transfer from **1–4** to **J61**. Efficient hole transfer from **J52** to **4** and electron transfer from **4** to **J52** have also been revealed by the PL quenching studies in the **J52:4** blend film (Fig. S8e, f).

Table S6 Excitation wavelengths of thin films for PL quenching studies.

Thin film	λ_{ex} / nm	Thin film	λ_{ex} / nm
J61	560	J52	550
1	560	2	580
3	630	4	650
J61:1^a	560	J61:1^b	560
J61:2^a	560	J61:2^b	580
J61:3^a	560	J61:3^b	630
J61:4^a	560	J61:4^b	650
J52:4^a	550	J52:4^b	650

^a Excitation at the absorption maximum of the thermally annealed pristine polymer donor (**J61** and **J52**) thin film for photoinduced electron transfer studies. ^b Excitation at the absorption maximum of the thermally annealed pristine electron acceptor (**1–4**) thin film for photoinduced hole transfer studies.

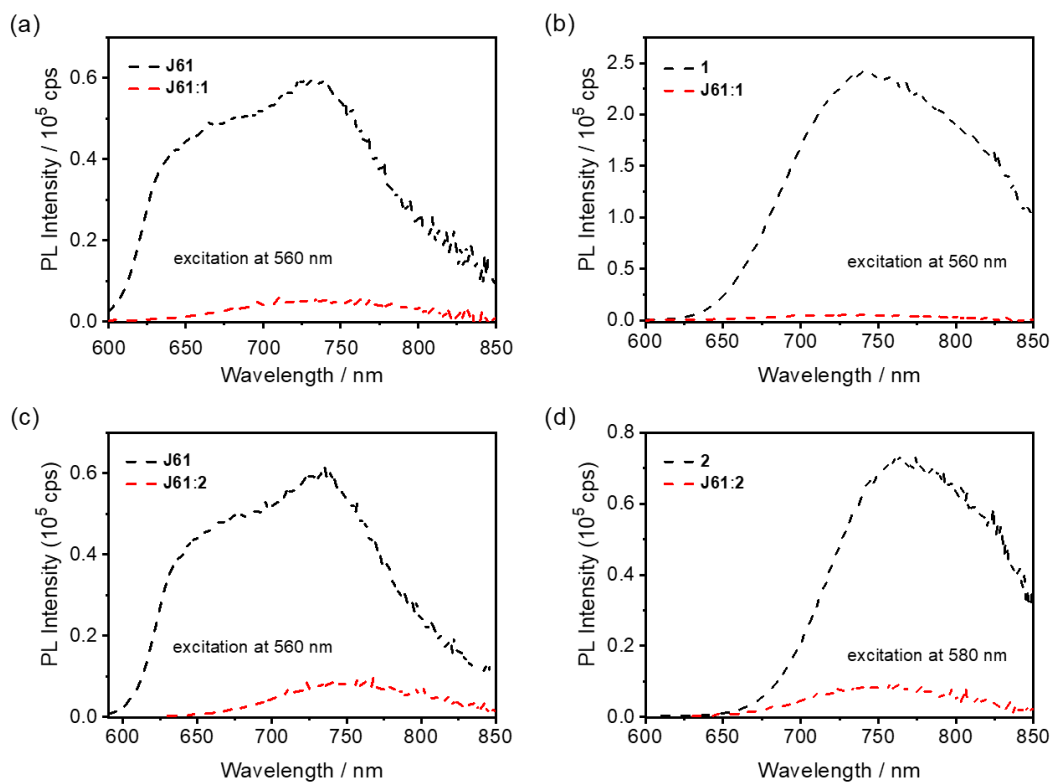


Fig. S7 PL spectra of (a–d) the thermally annealed pristine **J61**, **1** and **2** thin films, and the thermally annealed **J61:1** and **J61:2** blend thin films.

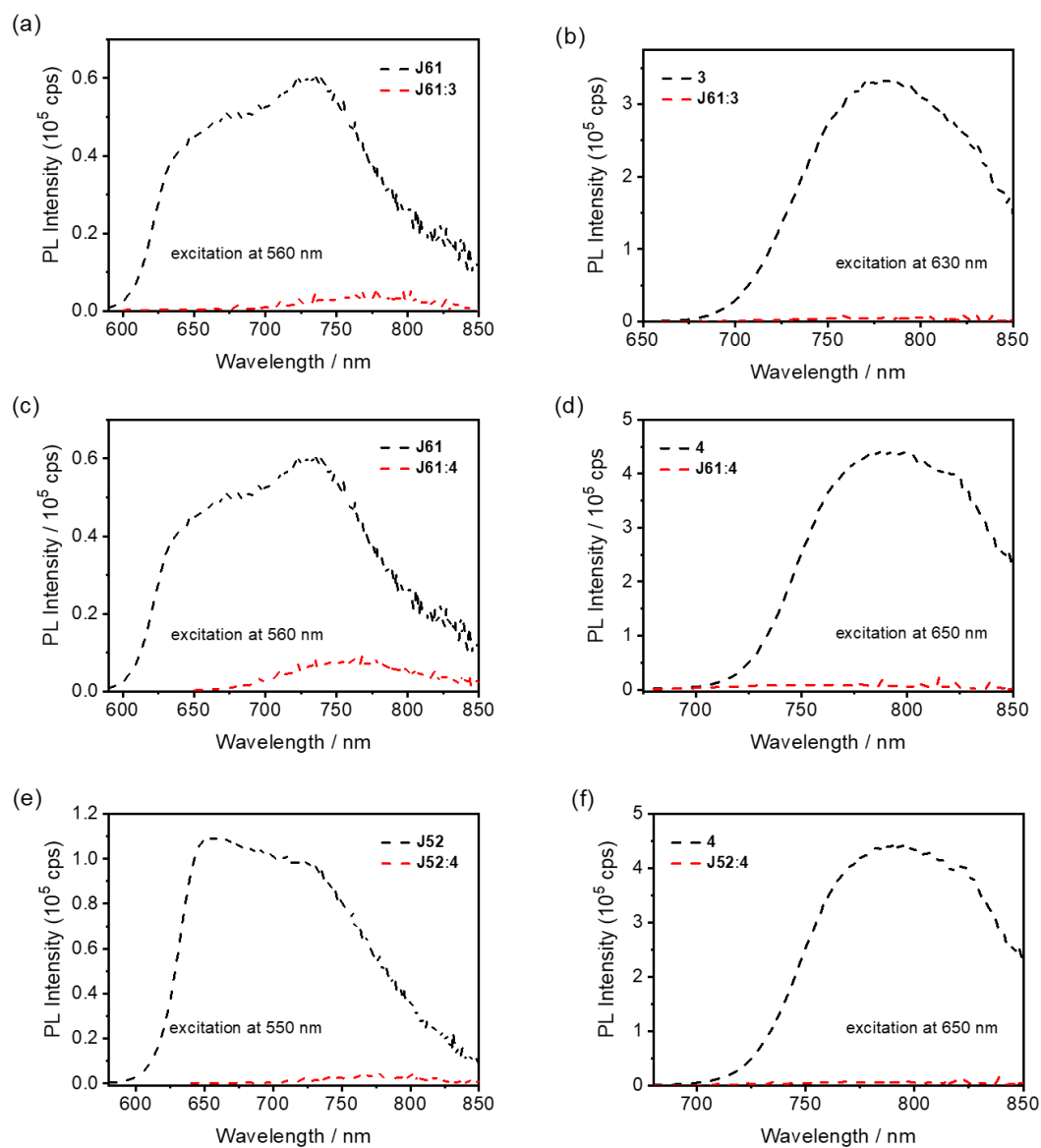


Fig. S8 PL spectra of (a–f) the thermally annealed pristine **J61**, **J52**, **3** and **4** thin films, and the thermally annealed **J61:3**, **J61:4** and **J52:4** blend thin films.

Atomic Force Microscopy (AFM) Studies. AFM experiments were performed on an Asylum Research MFP-3D Stand Alone Atomic Force Microscope in tapping mode under ambient conditions. The microscope was equipped with an All-Digital ARC2 Controller. The blend film was prepared under the same thermal annealing condition as the corresponding OSC devices.

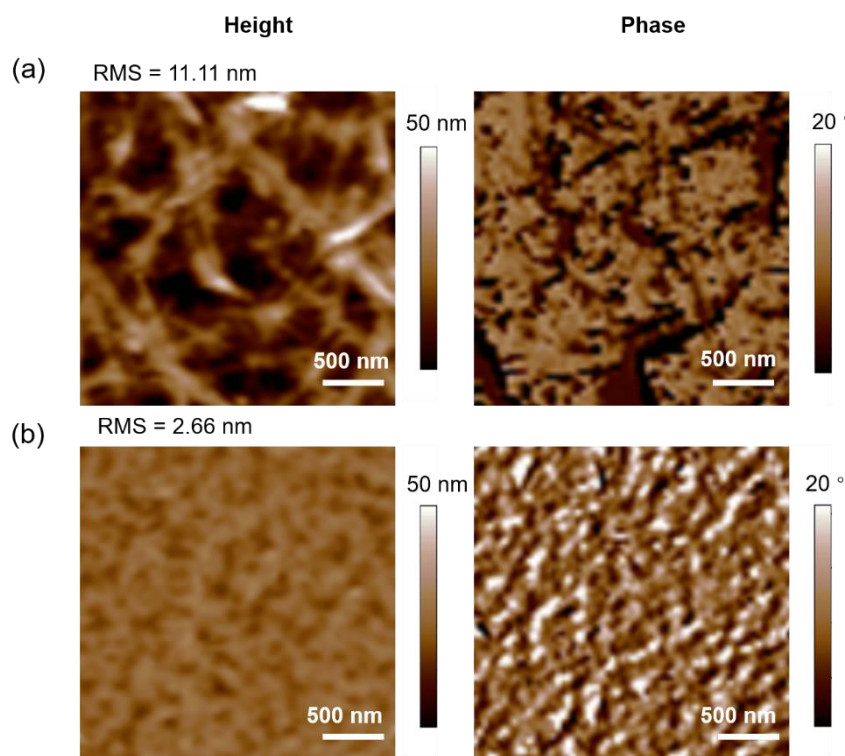


Fig. S9 AFM height and phase images of (a) the as-cast and (b) thermally annealed **J52:4** blend films.

Organic Resistive Memory Device Fabrication and Characterization. The schematic diagram of the resistive memory structure is illustrated in Fig. S10, in which the spin-coated active layer of the boron compound is sandwiched between an ITO bottom electrode and a vacuum-deposited aluminum top electrode. The ITO-coated glass substrate was pre-cleaned by sonicating successively with deionized water, acetone, isopropanol and absolute ethanol for 15 minutes each. Chloroform solutions of the boron(III) β -diketonate compound (*ca.* 10 mg mL⁻¹) were spin-coated onto the ITO substrate. Each organic layer was deposited with an aluminum top electrode by thermal evaporation through a shadow mask under a pressure of around 5×10^{-6} mbar. Device with active area of about 0.25 mm² was obtained. Current–voltage (I – V) characteristics of the memory devices were measured with a programmable Keithley model 4200-SCS power source in a probe station under ambient conditions. Cross-section scanning electron microscopy (SEM) experiments for the memory devices were performed on a Hitachi S-4800 FEG scanning electron microscope at the Electron Microscope Unit of The University of Hong Kong.

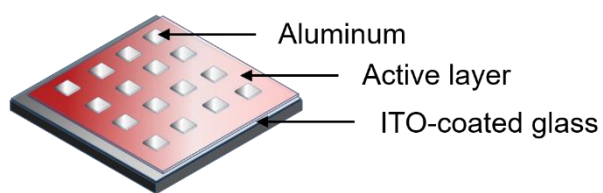


Fig. S10 Schematic diagram of the resistive memory configuration.

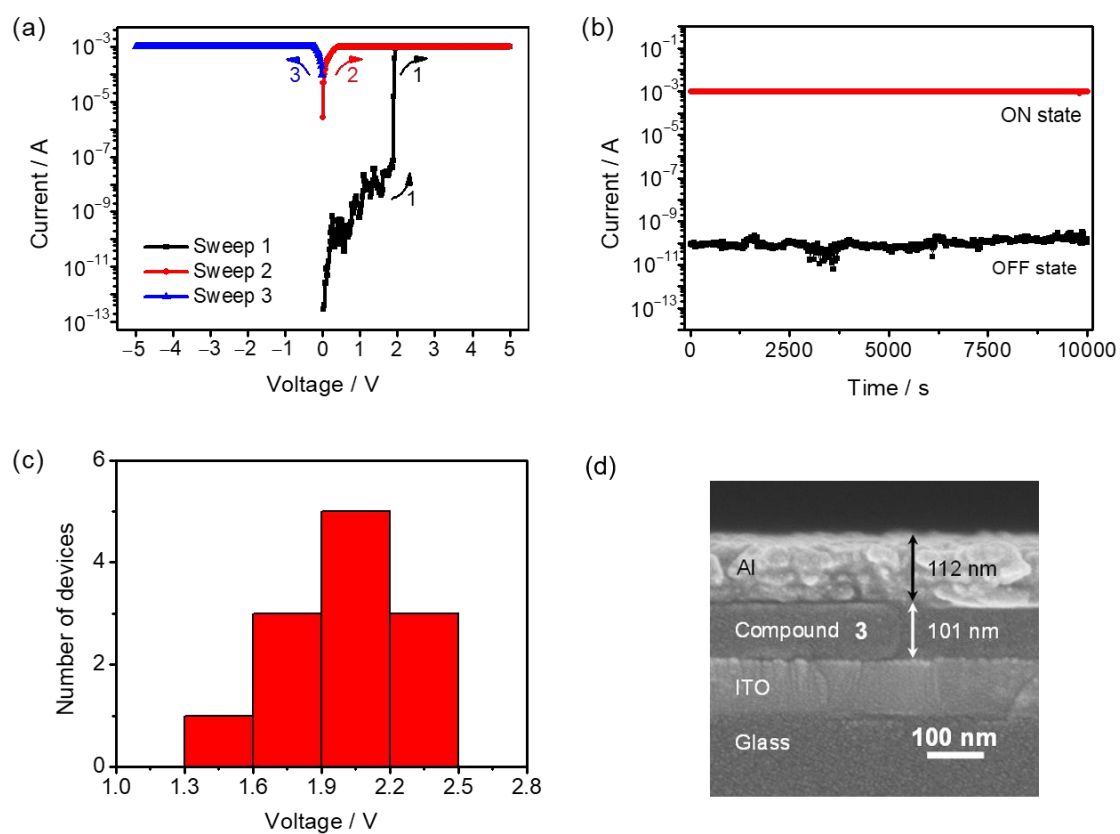


Fig. S11 (a) $I-V$ characteristics, (b) retention time in “OFF” and “ON” states under a constant bias of 1 V, (c) distribution of the switching threshold voltage (12 devices) and (d) SEM image of the cross-section of the memory device fabricated with compound 3.

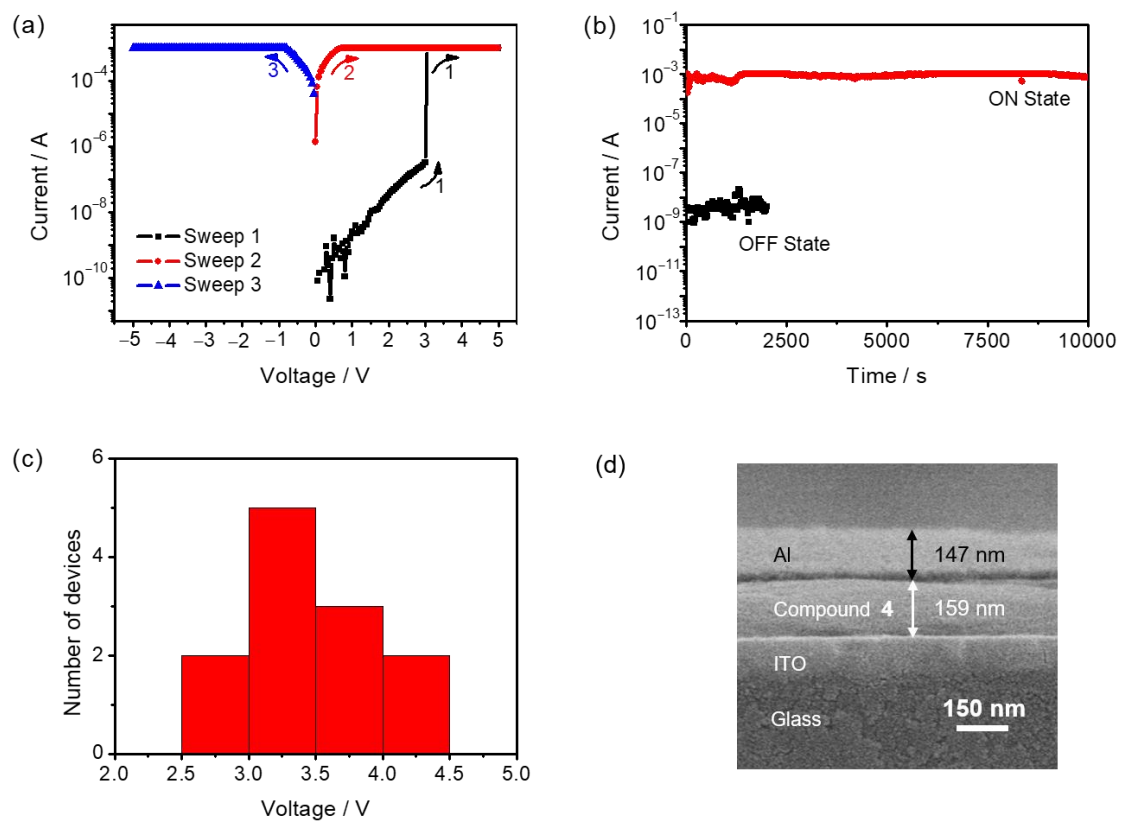


Fig. S12 (a) $I-V$ characteristics, (b) retention time in “OFF” and “ON” states under a constant bias of 1V, (c) distribution of the switching threshold voltage (12 devices) and (d) SEM image of the cross-section of the memory device fabricated with compound 4.

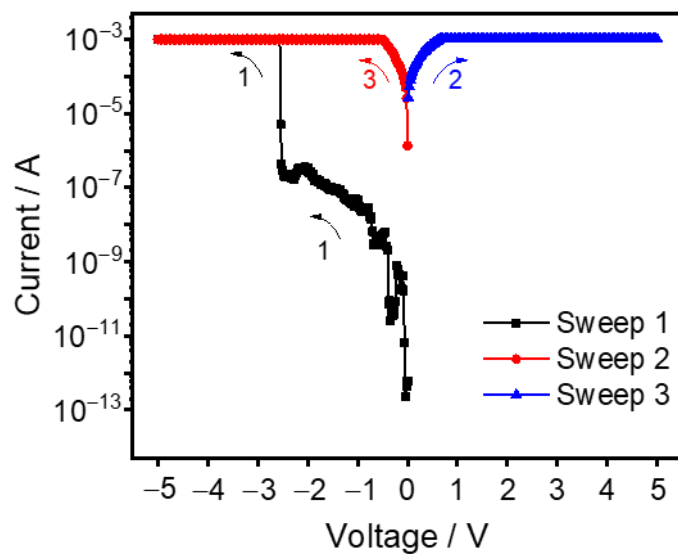


Fig. S13 I - V characteristics of the memory device fabricated with compound **1** with an initial reverse voltage sweep.

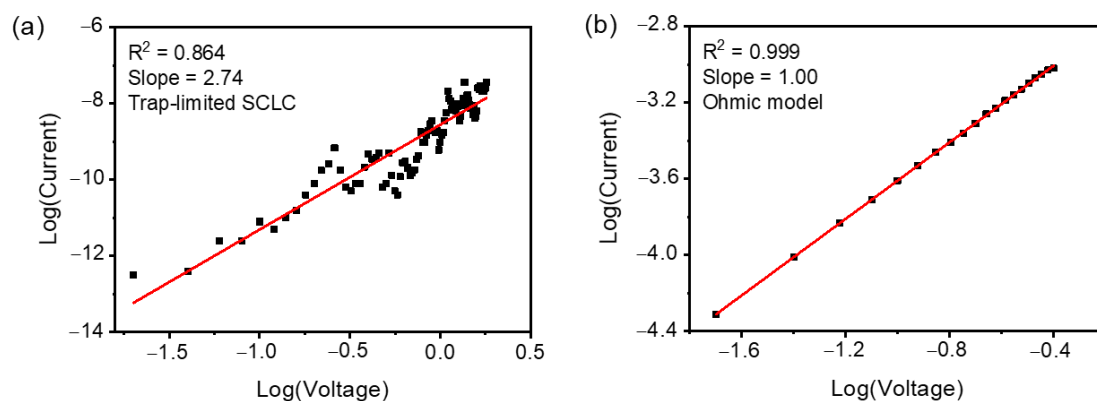


Fig. S14 Plots of $\log(I)$ vs. $\log(V)$ using the I - V characteristics of (a) the “OFF” state (from 0.02 to 1.80 V) and (b) the “ON” state (from 0.02 to 0.40 V) of the device fabricated with **3**.

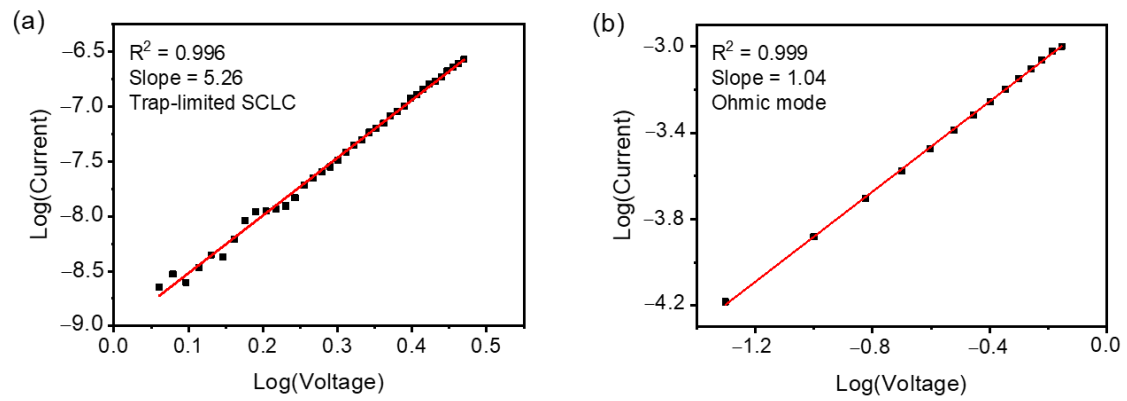


Fig. S15 Plots of $\log(I)$ vs. $\log(V)$ using the I - V characteristics of (a) the "OFF" state (from 1.15 to 2.95 V) and (b) the "ON" state (from 0.05 to 0.70 V) of the device fabricated with 4.

Table S7 Device performances of some recently reported organic resistive memories.⁴⁻¹⁰

Active materials	Retention time / s	V_{th} / V	ON/OFF ratio	Reference
Alkynylgold(III) organometallic complex	> 10000	2.2–2.8	10^5	4
Boron(III)-based small molecule	> 10000	2.8–3.4	10^6	5
Thiadizoloquinoxaline- based molecule	> 2000	1.9 (range not mentioned)	10^3	6
Pyrene-based molecule	> 7500	1.5–2.0	10^4	7
Ferrocene-based polymer	Not mentioned	1.5–2.2	10^3	8
Phosphole-based small molecule	> 10000	2.0–2.8	10^7	9
Al(III) metal complex	> 10000	3.6 (range not mentioned)	10^6	10
1	> 10000	1.1–2.7	10^6	This work
3	> 10000	1.3–2.5	10^6	This work
4	> 2000	2.5–4.5	10^6	This work

Computational Details and Studies

Computational Details. All calculations were carried out with the Gaussian 09 program suite.¹¹ The ground state (S_0) geometries of the model compounds of **1–4**, in which all the hexyl and octyl groups are replaced by methyl groups (labelled as **1'–4'**) were fully optimized in CH_2Cl_2 by density functional theory (DFT) with the hybrid Perdew, Burke, and Ernzerhof (PBE0) functional,^{12–14} in conjunction with the conductor-like polarizable continuum model (CPCM).^{15,16} On the basis of the optimized S_0 geometries, time-dependent DFT (TDDFT)^{17–19} calculations at the same level associated with CPCM (CH_2Cl_2) were performed to compute the singlet–singlet transitions. Vibrational frequency calculations were performed on all stationary points to verify that each was a minimum (NIMAG = 0) on the potential energy surface. For all the calculations, the 6-31G(d,p) basis set^{20–22} was applied for all atoms. All the DFT and TDDFT calculations were performed with a pruned (99,590) grid for numerical integration.

Computational Studies. In order to provide deeper understanding of the electronic structures, photophysical and electrochemical properties of these small molecules, DFT and TDDFT calculations have been performed on the model compounds of **1–4** (labelled as **1'–4'**), in which all the hexyl and octyl groups are replaced by methyl groups to reduce computational cost. The optimized ground-state geometries of **1'–4'** are illustrated in Fig. S16, and their Cartesian coordinates are presented in Tables S8–S11. In general, the calculated bond lengths and angles are in good agreement with that observed in the X-ray crystal structure of **1**. Generally, the compounds are found to have high planarity over the whole structure, with torsion angles of less than 25° between adjacent aromatic rings. The dipole moments of **1'–4'** are calculated to be 15.45, 12.70, 0.88 and 0.84 D, respectively. The details of the first twenty singlet–singlet transitions of **1'–4'**, obtained from the TDDFT/CPCM calculations, are summarized in Table S12. The simulated UV–vis absorption spectra and selected

frontier molecular orbitals of **1'**–**4'** are shown in Fig. S17–S21 and S22–S25, respectively. The low-energy absorption bands of **1'**–**4'** are found to correspond to the $S_0 \rightarrow S_1$ transition associated with the HOMO→LUMO excitation. The HOMOs of **1'**–**4'** are the π orbitals predominantly localized on the central fluorene or the IDT moiety, whereas the LUMOs are the π^* orbitals mainly localized on the boron(III) β -diketonate moieties, respectively. The low-energy absorption bands of **1'**–**4'**, which are red-shifted in energy from **1'** (576 nm) to **2'** (593 nm) to **3'** (630 nm) to **4'** (646 nm), can therefore be assigned predominantly to the ICT transition from the fluorene-based moiety (**1'** and **2'**) or IDT-based moiety (**3'** and **4'**) to the difluoroboron(III) β -diketonate-based moieties, which is in agreement with the trend observed and the spectral assignments. The orbital energy diagram showing the energies of the frontier molecular orbitals is illustrated in Fig. S26. The HOMO–LUMO gaps of the compounds are found to be in the trend of **1'** (2.59 eV) > **2'** (2.52 eV) > **3'** (2.43 eV) > **4'** (2.37 eV), in agreement with the experimental result from electrochemical studies.

To investigate the electron density distribution in the compounds, the electrostatic potential (ESP) surfaces of **1'**–**4'** are illustrated in Fig. S16. The electron density distribution is found to be not significantly affected by the replacement of the fluorene-centered donor moiety (**1'** and **2'**) by the IDT-centered moiety (**3'** and **4'**). On the other hand, by substituting the trifluoromethyl groups in **1'** and **3'** with the cyano groups in **2'** and **4'**, the electron density of the terminal boron(III) β -diketonate moieties is found to be reduced. Such lower electron density could lead to a stronger charge trapping property of the terminal boron(III) β -diketonate moieties, supportive of the relatively larger V_{th} for memory devices made with **4** as compared to those with **3**.

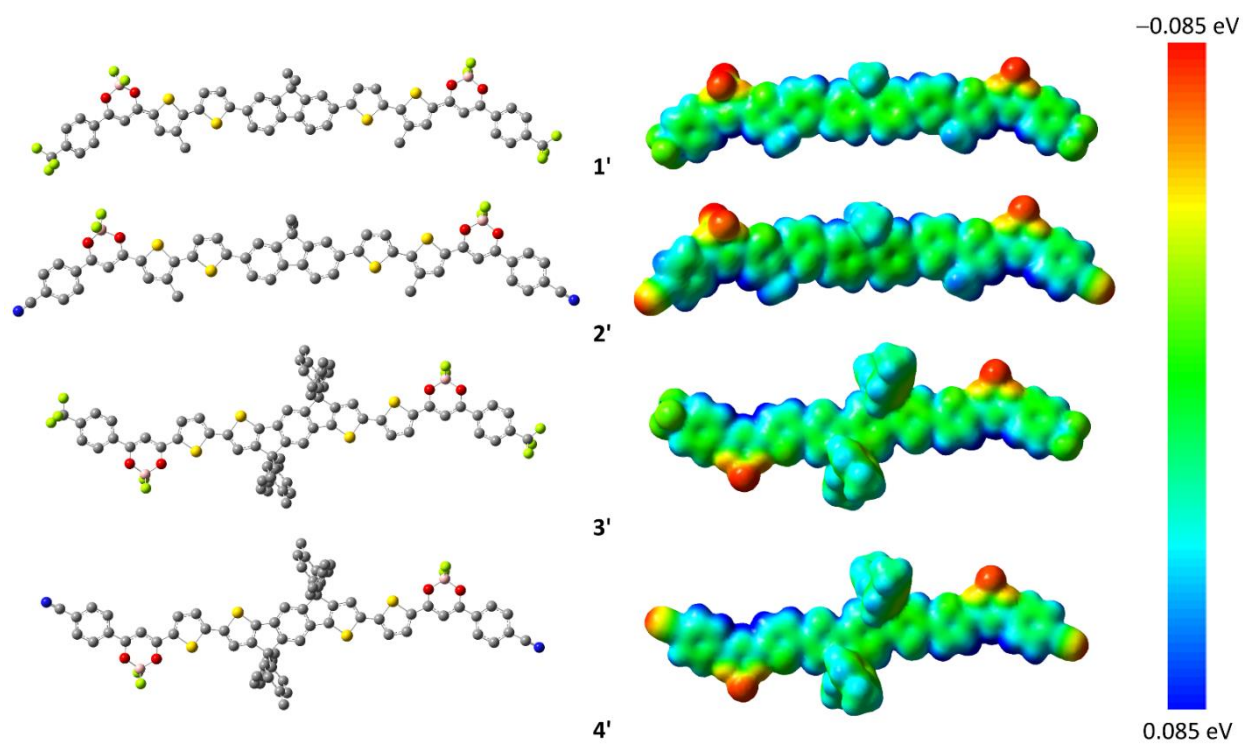


Fig. S16 Optimized structures of the ground state geometries of **1'**–**4'** at the PBE0 level of theory (all hydrogen atoms are omitted for clarity) (left) and their isosurfaces of the molecular electrostatic potential (right).

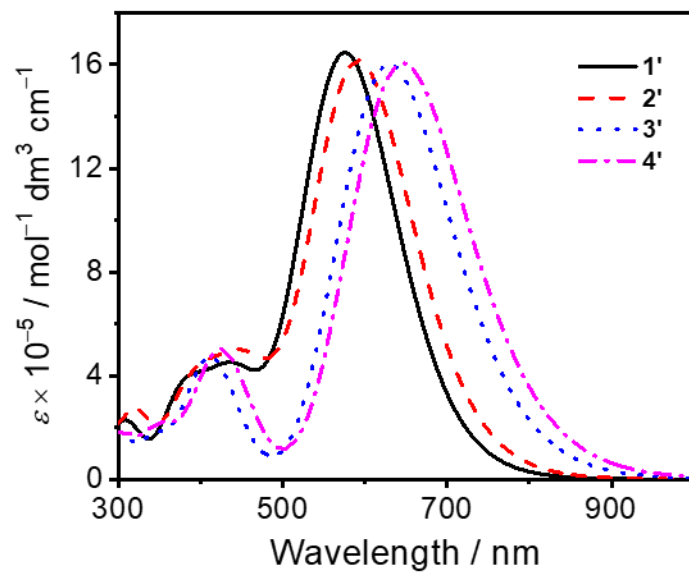


Fig. S17 Simulated absorption spectra of **1'**–**4'** at the PBE0 level in dichloromethane.

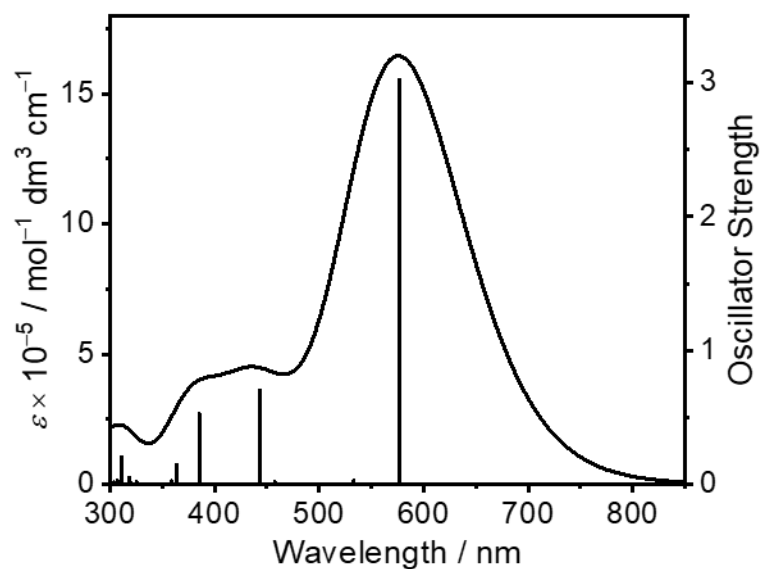


Fig. S18 Comparison of the TDDFT results for compound **1'** with the experimental electronic absorption spectrum. The heights of the vertical straight lines are the calculated oscillator strengths of the corresponding vertical transitions.

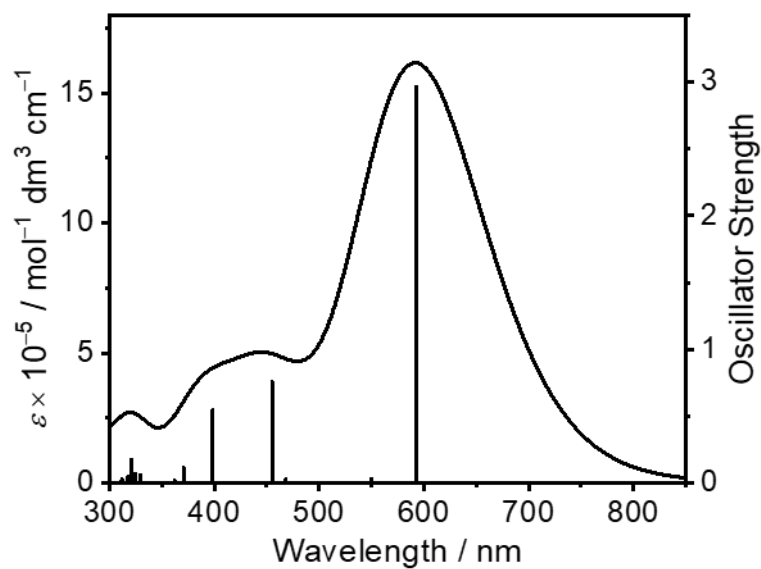


Fig. S19 Comparison of the TDDFT results for compound **2'** with the experimental electronic absorption spectrum. The heights of the vertical straight lines are the calculated oscillator strengths of the corresponding vertical transitions.

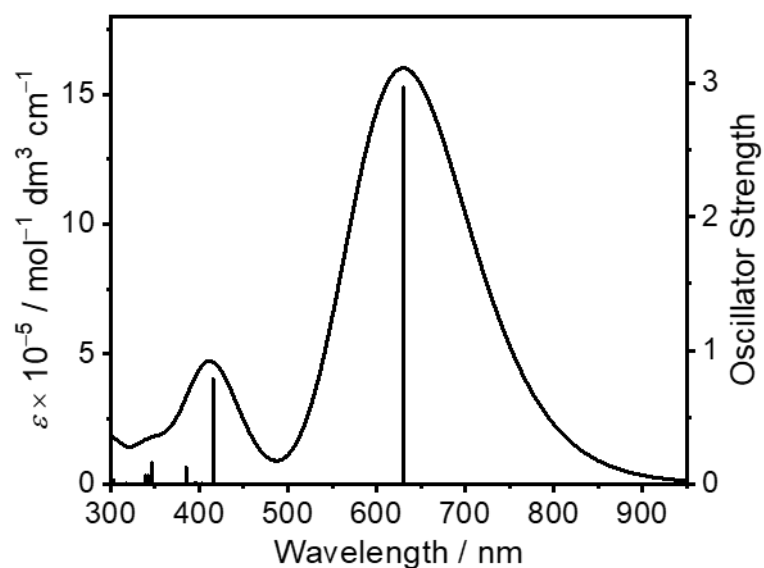


Fig. S20 Comparison of the TDDFT results for compound **3'** with the experimental electronic absorption spectrum. The heights of the vertical straight lines are the calculated oscillator strengths of the corresponding vertical transitions.

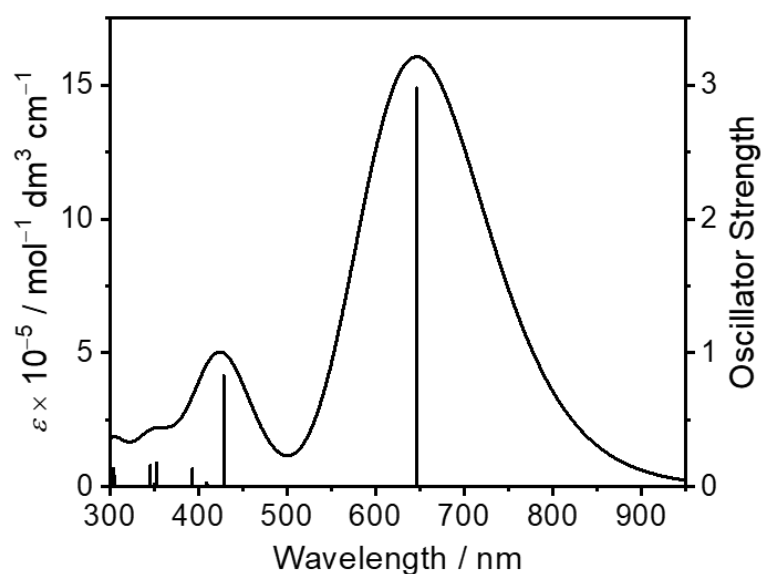


Fig. S21 Comparison of the TDDFT results for compound **4'** with the experimental electronic absorption spectrum. The heights of the vertical straight lines are the calculated oscillator strengths of the corresponding vertical transitions.

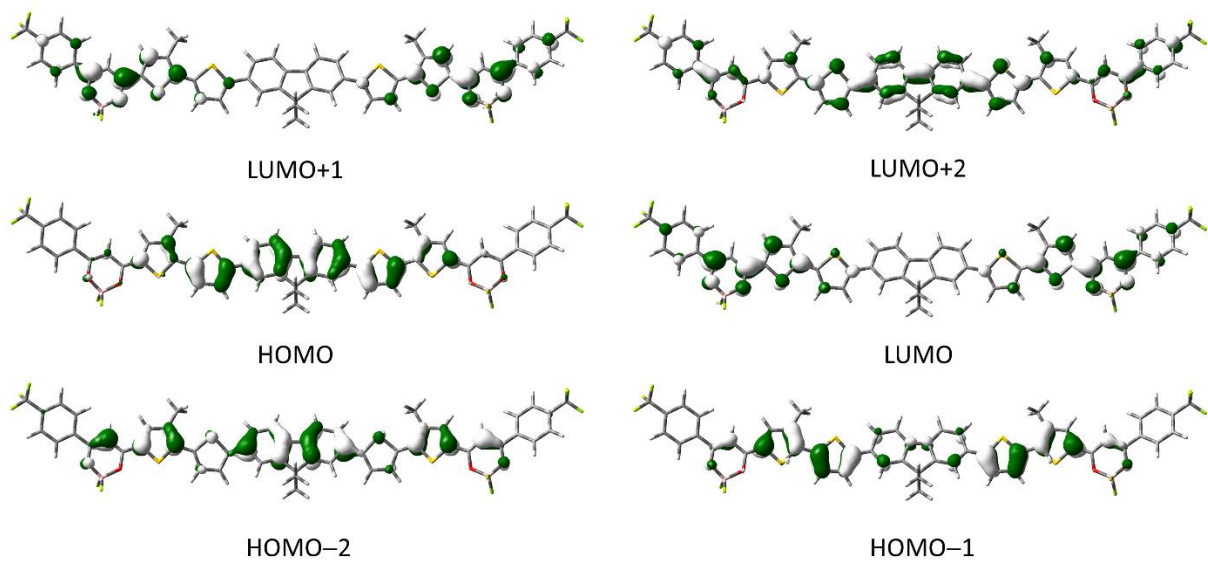


Fig. S22 Spatial plots (isovalue = 0.03) of selected frontier molecular orbitals of compound **1'** obtained from the PBE0/CPCM (dichloromethane) calculation.

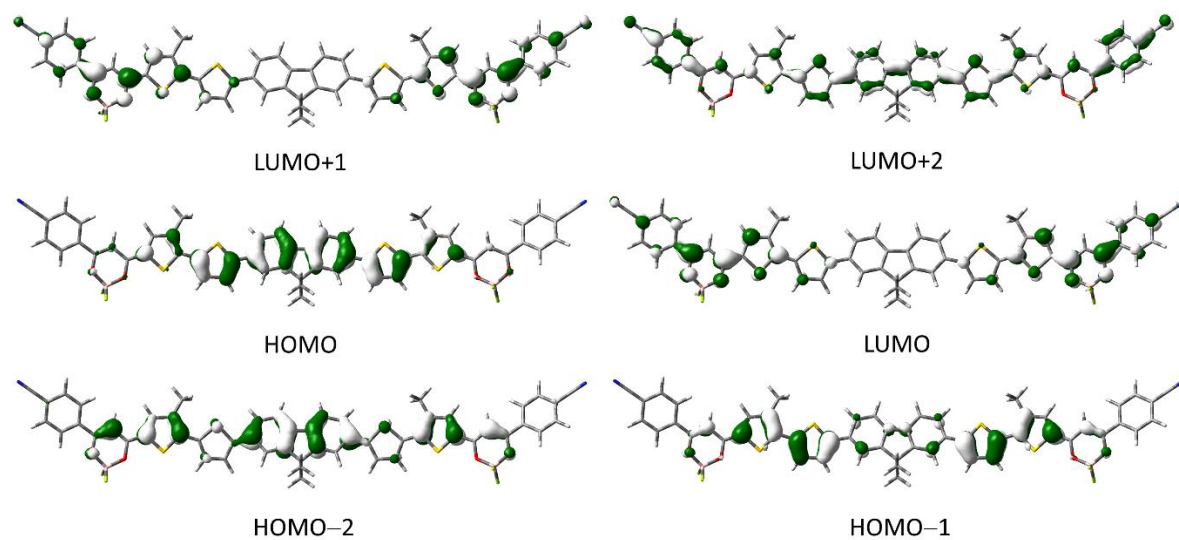


Fig. S23 Spatial plots (isovalue = 0.03) of selected frontier molecular orbitals of compound **2'** obtained from the PBE0/CPCM (dichloromethane) calculation.

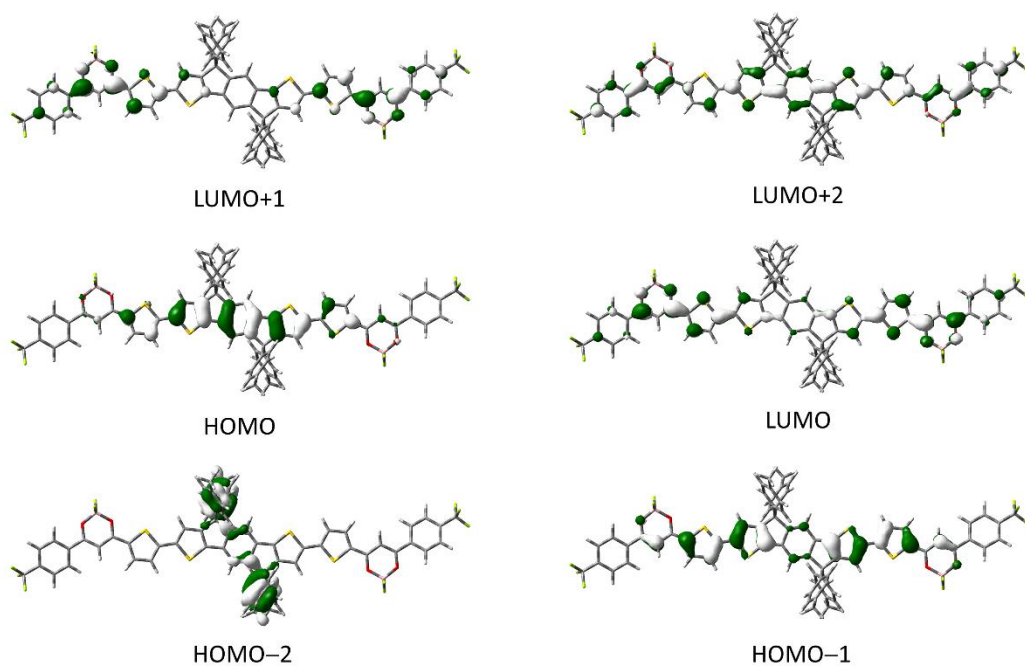


Fig. S24 Spatial plots (isovalue = 0.03) of selected frontier molecular orbitals of compound 3' obtained from the PBE0/CPCM (dichloromethane) calculation.

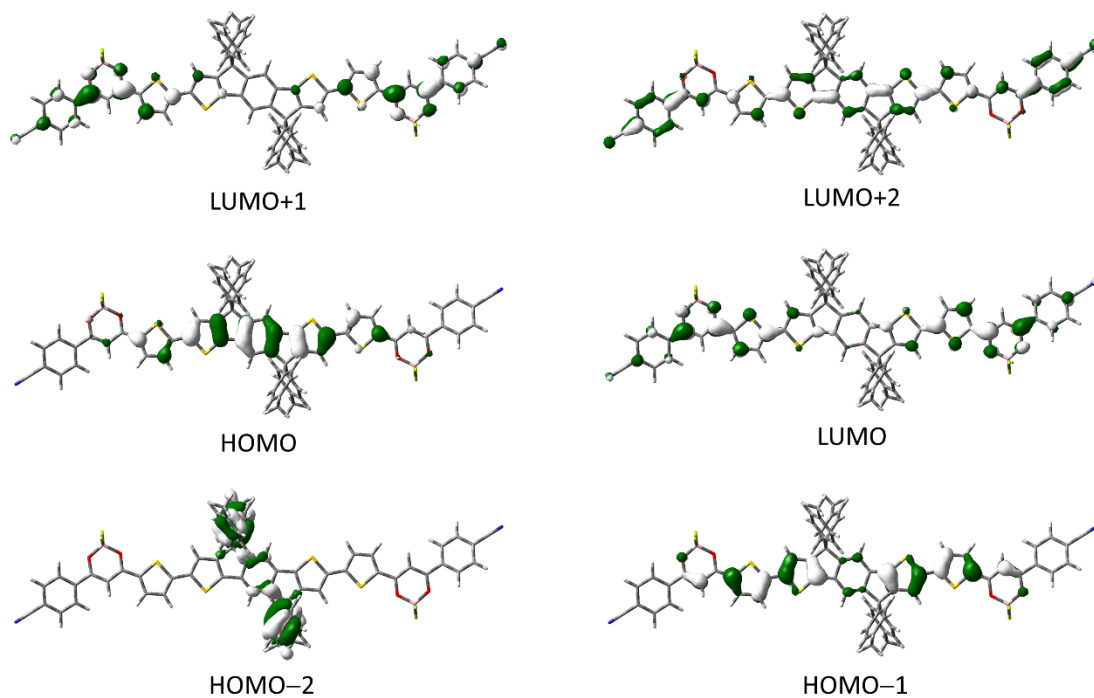


Fig. S25 Spatial plots (isovalue = 0.03) of selected frontier molecular orbitals of compound 4' obtained from the PBE0/CPCM (dichloromethane) calculation.

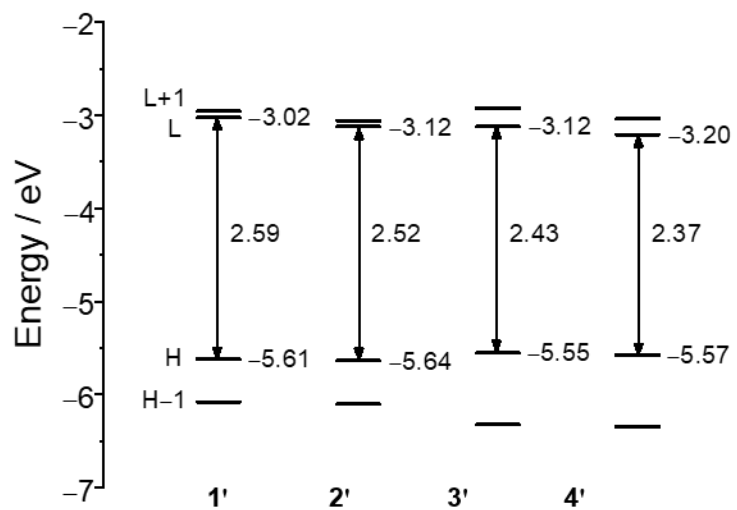


Fig. S26 Orbital energy diagram of the frontier molecular orbitals (H = HOMO and L = LUMO) of compounds **1'**–**4'**.

Table S8 Cartesian coordinates of the ground-state geometry of **1'** optimized at the PBE0 level.

1	C	1.170784	-1.216	-0.53591	55	S	-6.06468	0.466216	-0.64461
2	C	0.729307	0.019354	-1.04395	56	C	-4.89345	-0.8074	-0.75458
3	C	1.652087	0.99157	-1.42813	57	C	-5.51893	-2.03779	-0.72752
4	H	1.326613	1.948105	-1.82656	58	H	-4.98247	-2.97551	-0.81181
5	C	3.007629	0.717405	-1.3068	59	C	-6.91849	-1.95363	-0.62876
6	H	3.728813	1.462724	-1.63098	60	H	-7.56777	-2.8225	-0.61794
7	C	3.463734	-0.51271	-0.79855	61	C	-7.39682	-0.65604	-0.57601
8	C	2.520975	-1.48252	-0.40712	62	S	-9.96595	-1.44999	-0.0971
9	H	2.859666	-2.42531	0.013423	63	B	-14.1229	-2.56853	0.423005
10	S	9.941449	-1.41473	0.130796	64	F	-14.3992	-3.13672	-0.7981
11	S	6.057322	0.47845	-0.55196	65	F	-14.1385	-3.47398	1.448735
12	F	14.28342	-3.65082	0.488874	66	O	-12.7602	-1.94929	0.36564
13	F	13.93733	-2.57271	2.475822	67	O	-15.141	-1.51443	0.706578
14	O	15.13912	-1.51128	0.780027	68	C	-8.77112	-0.24286	-0.45278
15	O	12.73759	-1.91896	0.582379	69	C	-9.34497	1.027348	-0.58071
16	B	14.03244	-2.45739	1.109059	70	C	-10.7379	0.985096	-0.39985
17	C	4.889949	-0.79787	-0.6733	71	H	-11.3593	1.871167	-0.46714
18	C	5.517302	-2.02691	-0.6323	72	C	-11.2398	-0.27655	-0.13659
19	H	4.984026	-2.96596	-0.7219	73	C	-12.5917	-0.68781	0.096196
20	C	6.915342	-1.93973	-0.51371	74	C	-13.6747	0.203076	0.069997
21	H	7.566928	-2.80667	-0.49247	75	H	-13.5183	1.239436	-0.1867
22	C	7.389942	-0.64098	-0.4597	76	C	-14.9272	-0.25895	0.438754
23	C	8.760894	-0.22363	-0.31347	77	F	-20.6245	2.450457	1.475657
24	C	9.340609	1.039036	-0.4811	78	F	-20.029	3.424918	-0.3575
25	C	10.72843	1.002566	-0.26276	79	F	-19.3721	4.2161	1.541515
26	H	11.35541	1.881407	-0.36452	80	C	-16.1059	0.615604	0.565669
27	C	11.2191	-0.24605	0.074141	81	C	-15.9861	2.009437	0.64114
28	C	12.56273	-0.64844	0.363925	82	H	-15.0104	2.482482	0.636457
29	C	13.63919	0.250437	0.390269	83	C	-17.1169	2.803783	0.757169
30	H	13.46887	1.305838	0.243684	84	H	-17.0191	3.881535	0.828209
31	C	14.92108	-0.24915	0.549923	85	C	-18.3782	2.21142	0.800497
32	C	16.13016	0.58853	0.46908	86	C	-18.51	0.825777	0.734656
33	C	16.10506	1.866887	-0.10339	87	H	-19.4933	0.370089	0.777006
34	H	15.19158	2.263514	-0.53242	88	C	-17.3781	0.032034	0.621994
35	C	17.26091	2.631217	-0.15973	89	H	-17.4683	-1.04694	0.571739
36	H	17.2404	3.615303	-0.615	90	C	-19.6037	3.076716	0.870605
37	C	18.45297	2.123329	0.354561	91	C	-8.6087	2.295566	-0.88338
38	C	18.49269	0.849621	0.918569	92	H	-7.9384	2.582042	-0.06565
39	H	19.42477	0.45631	1.309687	93	H	-9.31587	3.114409	-1.03167

40	C	17.33692	0.084592	0.971112	94	C	8.615181	2.29239	-0.86203
41	H	17.3562	-0.90812	1.405915	95	H	9.328636	3.096768	-1.0534
42	C	19.69055	2.973998	0.34358	96	H	8.012993	2.154732	-1.76583
43	F	19.7043	3.822398	-0.69644	97	C	-0.00502	-2.10928	-0.17489
44	F	19.78215	3.720292	1.4594	98	C	-0.01753	-2.43757	1.325409
45	F	20.80663	2.232078	0.276186	99	H	0.865722	-3.02472	1.596152
46	C	-1.1764	-1.21846	-0.55588	100	H	-0.02359	-1.52552	1.928879
47	C	-0.72896	0.017836	-1.05636	101	C	0.003471	-3.4051	-0.99917
48	C	-1.64707	0.988187	-1.45619	102	H	0.012157	-3.19072	-2.07158
49	H	-1.31681	1.945156	-1.84962	103	H	0.887446	-4.00478	-0.76003
50	C	-3.00394	0.711555	-1.35722	104	H	-0.90417	-3.02642	1.580947
51	H	-3.72115	1.455413	-1.69333	105	H	-0.88281	-4.00707	-0.7748
52	C	-3.46597	-0.51943	-0.8565	106	H	-8.00263	2.206972	-1.79089
53	C	-2.52805	-1.48763	-0.4498	107	H	7.94277	2.630553	-0.06604
54	H	-2.87208	-2.43108	-0.03507					

Table S9 Cartesian coordinates of the ground-state geometry of **2'** optimized at the PBE0 level.

1	C	1.173106	-0.93186	-0.55145	53	C	-5.51758	-1.73234	-0.7724
2	C	0.731224	0.33547	-0.97307	54	H	-4.98222	-2.66228	-0.92337
3	C	1.653752	1.330393	-1.29468	55	C	-6.91621	-1.65426	-0.66123
4	H	1.328015	2.311921	-1.62653	56	H	-7.566	-2.52165	-0.70652
5	C	3.009327	1.047292	-1.19735	57	C	-7.39314	-0.36287	-0.51627
6	H	3.729997	1.812294	-1.47323	58	S	-9.96499	-1.18862	-0.11252
7	C	3.465885	-0.21457	-0.77435	59	B	-14.1259	-2.3367	0.321187
8	C	2.523373	-1.20767	-0.44567	60	F	-14.401	-2.8225	-0.93468
9	H	2.862086	-2.17707	-0.09075	61	F	-14.1421	-3.30769	1.285009
10	S	9.942171	-1.17454	0.091967	62	O	-12.7623	-1.7156	0.30564
11	S	6.062279	0.756815	-0.48441	63	O	-15.1444	-1.30347	0.673038
12	F	14.28208	-3.43114	0.356617	64	C	-8.76616	0.041412	-0.3595
13	F	13.93629	-2.4399	2.388538	65	C	-9.33627	1.320295	-0.37556
14	O	15.14117	-1.30772	0.741624	66	C	-10.7289	1.266759	-0.19989
15	O	12.73857	-1.70262	0.525035	67	H	-11.347	2.157562	-0.18861
16	B	14.03282	-2.26616	1.028497	68	C	-11.2351	-0.01198	-0.04854
17	C	4.892115	-0.50855	-0.67314	69	C	-12.5874	-0.43696	0.146922
18	C	5.517533	-1.73905	-0.70642	70	C	-13.6683	0.458013	0.196276
19	H	4.982264	-2.67058	-0.84753	71	H	-13.5076	1.511904	0.029199
20	C	6.916046	-1.66111	-0.58968	72	C	-14.9229	-0.031	0.513984
21	H	7.566205	-2.52877	-0.62209	73	C	-16.1023	0.83314	0.702261
22	C	7.393167	-0.36816	-0.4633	74	C	-15.9802	2.214192	0.905959
23	C	8.765026	0.038166	-0.29882	75	H	-15.0036	2.6822	0.958232
24	C	9.347923	1.306085	-0.41048	76	C	-17.1076	3.00089	1.074789
25	C	10.73523	1.256283	-0.19543	77	H	-17.0119	4.068464	1.238399
26	H	11.36435	2.137174	-0.25894	78	C	-18.3769	2.407908	1.04228
27	C	11.22302	-0.00783	0.085676	79	C	-18.5097	1.027115	0.846968
28	C	12.5647	-0.42479	0.357795	80	H	-19.495	0.574904	0.824026
29	C	13.64417	0.471141	0.419841	81	C	-17.3758	0.248767	0.682767
30	H	13.47583	1.53189	0.315724	82	H	-17.4652	-0.82048	0.530171
31	C	14.92309	-0.03738	0.56216	83	C	-8.59592	2.608054	-0.56338
32	C	16.13424	0.80185	0.519921	84	H	-7.91874	2.813432	0.272833
33	C	16.11261	2.101556	-0.00345	85	H	-9.30031	3.439927	-0.62938
34	H	15.20159	2.515423	-0.4208	86	C	8.625305	2.576711	-0.73529
35	C	17.26543	2.868922	-0.02352	87	H	9.340962	3.385552	-0.89725
36	H	17.24935	3.872264	-0.43415	88	H	8.0176	2.47852	-1.64049
37	C	18.4595	2.338112	0.482651	89	C	-0.00237	-1.84685	-0.24853
38	C	18.49391	1.03686	1.000368	90	C	-0.00969	-2.27907	1.22516
39	H	19.42175	0.632011	1.389153	91	H	0.873847	-2.88461	1.450669

40	C	17.33626	0.276303	1.012381	92	H	-0.01235	-1.41149	1.891004
41	H	17.3495	-0.73138	1.411165	93	C	0.001438	-3.08196	-1.1613
42	C	-1.17404	-0.93074	-0.56255	94	H	0.006591	-2.79317	-2.21613
43	C	-0.72704	0.336371	-0.97943	95	H	0.885433	-3.69786	-0.96781
44	C	-1.64543	1.332897	-1.30798	96	H	-0.8961	-2.88351	1.442182
45	H	-1.31547	2.314233	-1.63623	97	H	-0.88492	-3.69705	-0.97625
46	C	-3.00221	1.051668	-1.22224	98	H	-7.99647	2.602684	-1.47955
47	H	-3.71982	1.817642	-1.50333	99	H	7.958798	2.884287	0.077871
48	C	-3.46372	-0.21031	-0.80512	100	C	19.65083	3.129869	0.465675
49	C	-2.52556	-1.20517	-0.46954	101	C	-19.5434	3.217769	1.214722
50	H	-2.86914	-2.17439	-0.11874	102	N	20.61759	3.773865	0.452369
51	S	-6.05997	0.760527	-0.51375	103	N	-20.4905	3.875873	1.354135
52	C	-4.89103	-0.50321	-0.71726					

Table S10 Cartesian coordinates of the ground-state geometry of **3'** optimized at the PBE0 level.

1	S	7.789255	-1.28464	0.096174	70	C	2.306493	-4.46837	-3.67462
2	B	11.86818	-2.72881	0.325159	71	H	0.942609	-3.02722	-4.50124
3	F	11.93601	-3.07877	1.652974	72	H	3.644949	-5.70505	-2.52612
4	F	11.93651	-3.80637	-0.51509	73	C	2.435848	-5.27551	-4.93535
5	O	10.56735	-2.0265	0.081122	74	H	1.826283	-6.18533	-4.88422
6	O	13.00082	-1.80955	0.009543	75	H	2.105773	-4.70715	-5.80876
7	C	6.66829	0.03475	0.037509	76	H	3.470162	-5.59091	-5.10234
8	C	7.335226	1.254813	-0.00163	77	C	1.249433	-5.39695	4.849442
9	C	8.726705	1.121381	0.013569	78	H	0.258407	-5.85869	4.875184
10	H	9.406729	1.964337	-0.01881	79	H	1.986505	-6.20782	4.888817
11	C	9.1459	-0.19861	0.066983	80	H	1.374145	-4.79991	5.756952
12	C	10.4756	-0.729	0.099212	81	C	-2.02378	2.987502	1.36646
13	C	11.61903	0.083068	0.123281	82	C	-2.85378	4.114089	1.423713
14	H	11.5212	1.156439	0.174877	83	C	-1.34515	2.614579	2.526548
15	C	12.86402	-0.51542	0.022912	84	C	-2.99105	4.841952	2.598494
16	F	18.86214	1.6037	-0.62358	85	H	-3.3934	4.430713	0.535224
17	F	18.11793	2.918092	0.920225	86	C	-1.48465	3.349489	3.702427
18	F	17.78763	3.406776	-1.15718	87	H	-0.70024	1.74153	2.521106
19	C	14.12072	0.246237	-0.08082	88	C	-2.30509	4.476456	3.762409
20	C	14.13396	1.608199	-0.40906	89	H	-3.64334	5.71199	2.612469
21	H	13.21146	2.134714	-0.62708	90	H	-0.94168	3.035872	4.590824
22	C	15.33505	2.296411	-0.49183	91	C	-1.83382	3.026578	-1.1758
23	H	15.34175	3.347761	-0.75785	92	C	-2.45526	2.675753	-2.37589
24	C	16.53453	1.62859	-0.24909	93	C	-1.00496	4.153309	-1.16964
25	C	16.5352	0.271858	0.068813	94	C	-2.25932	3.430633	-3.52882
26	H	17.4718	-0.24482	0.248125	95	H	-3.09964	1.802381	-2.4157
27	C	15.3335	-0.41623	0.148306	96	C	-0.80962	4.902173	-2.32479
28	H	15.32202	-1.47188	0.39388	97	H	-0.51339	4.456279	-0.24943
29	C	17.82908	2.389172	-0.28275	98	C	-1.43611	4.559067	-3.52671
30	H	6.82409	2.209704	-0.04416	99	H	-2.75835	3.134681	-4.44857
31	C	5.250916	-0.19706	0.035468	100	H	-0.15906	5.772902	-2.29036
32	C	4.577253	-1.4082	0.035019	101	C	-2.43367	5.285512	5.021986
33	S	4.13475	1.157183	0.037286	102	H	-1.82121	6.193376	4.970575
34	C	3.183148	-1.24013	0.043196	103	H	-3.46722	5.604274	5.187218
35	H	5.086883	-2.36555	0.026172	104	H	-2.10645	4.71722	5.896522
36	C	2.797153	0.084256	0.043065	105	C	-1.25274	5.392171	-4.76366
37	C	1.968015	-2.15326	0.012428	106	H	-1.38042	4.794309	-5.67021
38	C	1.360235	0.209305	0.040383	107	H	-1.98821	6.204511	-4.80254
39	C	0.842268	-1.10815	0.019707	108	H	-0.26083	5.851875	-4.79187

40	C	0.523455	1.329372	0.062129	109	C	-6.66859	-0.03256	0.06996
41	C	-0.52382	-1.3268	0.030185	110	C	-7.33507	-1.25171	0.135081
42	C	-0.84265	1.110729	0.072205	111	S	-7.78999	1.285224	-0.01086
43	H	0.934279	2.334578	0.071003	112	C	-8.72667	-1.11886	0.121925
44	C	-1.36059	-0.20675	0.052428	113	H	-6.82341	-2.20549	0.193424
45	H	-0.93463	-2.33202	0.021512	114	C	-9.14632	0.200058	0.049173
46	C	-1.96844	2.155805	0.078702	115	H	-9.40603	-1.96199	0.162678
47	C	-2.79752	-0.08177	0.051538	116	C	-10.4761	0.730156	0.014632
48	C	-3.18357	1.242599	0.050049	117	C	-11.6205	-0.0773	0.090985
49	C	-4.5777	1.410617	0.060739	118	C	-12.8631	0.509667	-0.08046
50	C	-5.25123	0.199443	0.064437	119	H	-11.525	-1.14195	0.238567
51	H	-5.08744	2.367894	0.070208	120	O	-10.5664	2.020883	-0.11917
52	S	-4.13506	-1.15475	0.061975	121	O	-12.9994	1.797318	-0.20941
53	C	1.83271	-3.02597	1.265504	122	B	-11.8702	2.743866	0.028756
54	C	1.004317	-4.15302	1.256973	123	F	-11.9226	3.728658	-0.91998
55	C	2.45293	-2.67661	2.466666	124	F	-11.96	3.23	1.311464
56	C	0.808251	-4.90363	2.410883	125	C	-14.1184	-0.25932	-0.13769
57	H	0.513679	-4.45485	0.335893	126	C	-15.334	0.416671	0.027419
58	C	2.256277	-3.43323	3.61832	127	C	-14.1263	-1.64331	-0.35516
59	H	3.09689	-1.80302	2.508347	128	C	-16.5341	-0.27797	-0.01048
60	C	1.433528	-4.56201	3.61384	129	H	-15.326	1.487443	0.195563
61	H	0.158063	-5.77457	2.374624	130	C	-15.3257	-2.33816	-0.39667
62	H	2.754364	-3.1384	4.538931	131	H	-13.2002	-2.18424	-0.5147
63	C	2.024026	-2.98298	-1.27659	132	C	-16.5285	-1.65531	-0.22155
64	C	1.345469	-2.60869	-2.43627	133	H	-17.4724	0.247103	0.131459
65	C	2.854492	-4.10916	-1.33528	134	H	-15.3272	-3.40962	-0.56466
66	C	1.485552	-3.34186	-3.61319	135	C	-17.8273	-2.40298	-0.31979
67	H	0.700127	-1.73597	-2.4297	136	F	-18.2628	-2.46474	-1.59135
68	C	2.992336	-4.83527	-2.51106	137	F	-18.7974	-1.81747	0.398794
69	H	3.393977	-4.42688	-0.44709	138	F	-17.7084	-3.66778	0.114049

Table S11 Cartesian coordinates of the ground-state geometry of **4'** optimized at the PBE0 level.

1	S	7.832462	-0.97293	0.099555	68	H	3.872581	-5.5423	-2.57671
2	B	11.96466	-2.25409	0.349866	69	C	2.659964	-5.13876	-4.98876
3	F	12.04539	-2.58894	1.680453	70	H	2.081919	-6.06948	-4.94885
4	F	12.07456	-3.33487	-0.48122	71	H	2.315814	-4.57501	-5.85973
5	O	10.63747	-1.60411	0.099883	72	H	3.705588	-5.41682	-5.15153
6	O	13.06069	-1.29378	0.02602	73	C	1.464824	-5.37429	4.795885
7	C	6.660911	0.300916	0.028545	74	H	0.496416	-5.88205	4.814902
8	C	7.27946	1.546559	-0.01611	75	H	2.238906	-6.14998	4.833735
9	C	8.674528	1.468208	0.003422	76	H	1.557955	-4.77737	5.707256
10	H	9.320832	2.337101	-0.03243	77	C	-2.14528	2.891463	1.358614
11	C	9.145415	0.165566	0.06589	78	C	-3.01653	3.986127	1.421105
12	C	10.49371	-0.31175	0.103807	79	C	-1.45849	2.53415	2.518892
13	C	11.60589	0.54545	0.118103	80	C	-3.18582	4.698592	2.601205
14	H	11.46597	1.614723	0.157282	81	H	-3.56337	4.290322	0.532699
15	C	12.87154	-0.00614	0.025613	82	C	-1.63037	3.25346	3.700064
16	C	14.09938	0.80223	-0.08472	83	H	-0.7817	1.685594	2.509445
17	C	14.06093	2.161053	-0.42523	84	C	-2.49211	4.348909	3.765347
18	H	13.11933	2.651064	-0.6456	85	H	-3.86982	5.543846	2.619148
19	C	15.23176	2.895533	-0.51419	86	H	-1.0802	2.952658	4.588463
20	H	15.20095	3.945501	-0.78292	87	C	-1.95295	2.95536	-1.18373
21	C	16.46134	2.271885	-0.26312	88	C	-2.55359	2.58383	-2.38822
22	C	16.51169	0.912134	0.069896	89	C	-1.17555	4.118034	-1.16807
23	H	17.46668	0.435598	0.261651	90	C	-2.38834	3.35374	-3.53592
24	C	15.33517	0.1859	0.15337	91	H	-3.1576	1.682426	-2.43551
25	H	15.36088	-0.86633	0.411582	92	C	-1.01104	4.882252	-2.318
26	H	6.73098	2.480046	-0.06674	93	H	-0.70094	4.437191	-0.24446
27	C	5.254248	0.013294	0.022835	94	C	-1.61769	4.51867	-3.52401
28	C	4.629854	-1.22415	0.012898	95	H	-2.87029	3.040993	-4.4592
29	S	4.0845	1.321556	0.031718	96	H	-0.40081	5.781383	-2.27609
30	C	3.230482	-1.11241	0.019169	97	C	-2.65604	5.142028	5.03093
31	H	5.177531	-2.16012	-0.00232	98	H	-2.07478	6.07075	4.991135
32	C	2.791357	0.195566	0.026986	99	H	-3.7009	5.423678	5.192318
33	C	2.053513	-2.07377	-0.02029	100	H	-2.31474	4.577669	5.902632
34	C	1.350619	0.262177	0.021725	101	C	-1.46897	5.367153	-4.75513
35	C	0.886494	-1.07511	-0.00918	102	H	-1.5651	4.76965	-5.6658
36	C	0.469067	1.347209	0.04895	103	H	-2.24164	6.144292	-4.79202
37	C	-0.46955	-1.34917	-0.00402	104	H	-0.49965	5.873067	-4.77656
38	C	-0.88695	1.073148	0.05397	105	C	-6.66166	-0.30172	0.030388
39	H	0.838383	2.368241	0.065841	106	C	-7.28089	-1.54691	0.077346

40	C	-1.35113	-0.26415	0.023577	107	S	-7.83267	0.973095	-0.03184
41	H	-0.83885	-2.37021	-0.02066	108	C	-8.67604	-1.46754	0.064981
42	C	-2.05386	2.071894	0.065128	109	H	-6.73283	-2.48095	0.122076
43	C	-2.79191	-0.19745	0.020067	110	C	-9.14629	-0.16431	0.011005
44	C	-3.23087	1.110575	0.027736	111	H	-9.32255	-2.33653	0.093381
45	C	-4.63018	1.222558	0.03668	112	C	-10.4943	0.314931	-0.01554
46	C	-5.25482	-0.01476	0.0295	113	C	-11.6085	-0.53747	0.043105
47	H	-5.17756	2.158703	0.052078	114	C	-12.871	0.00691	-0.11356
48	S	-4.08532	-1.32323	0.019054	115	H	-11.473	-1.60069	0.168469
49	C	1.951639	-2.95862	1.227504	116	O	-10.6346	1.603046	-0.12393
50	C	1.174893	-4.12169	1.209738	117	O	-13.0578	1.290505	-0.21742
51	C	2.550645	-2.58797	2.433089	118	B	-11.9646	2.275648	0.033372
52	C	1.009453	-4.88717	2.358706	119	F	-12.0536	3.269824	-0.90221
53	H	0.701517	-4.44014	0.285254	120	F	-12.0715	2.74014	1.322309
54	C	2.384474	-3.35914	3.579798	121	C	-14.0984	-0.80688	-0.17962
55	H	3.15409	-1.68628	2.482032	122	C	-15.3362	-0.17559	0.001951
56	C	1.614486	-4.5245	3.56579	123	C	-14.0569	-2.18591	-0.42502
57	H	0.39975	-5.78659	2.315174	124	C	-16.5121	-0.90617	-0.04359
58	H	2.865164	-3.04707	4.50396	125	H	-15.364	0.892027	0.186285
59	C	2.146092	-2.89193	-1.31459	126	C	-15.2271	-2.92496	-0.47607
60	C	1.459663	-2.53392	-2.47485	127	H	-13.1129	-2.68897	-0.60158
61	C	3.01794	-3.9861	-1.37767	128	C	-16.4589	-2.2856	-0.2818
62	C	1.632505	-3.25204	-3.65662	129	H	-17.4689	-0.41798	0.104685
63	H	0.782353	-1.68578	-2.46491	130	H	-15.1941	-3.99088	-0.67186
64	C	3.188176	-4.69738	-2.55834	131	C	-17.6693	-3.04645	-0.33179
65	H	3.564422	-4.29089	-0.48925	132	C	17.67217	3.028471	-0.35172
66	C	2.494866	-4.34695	-3.72251	133	N	18.65511	3.643531	-0.42291
67	H	1.082574	-2.95074	-4.545	134	N	-18.6518	-3.665	-0.37167

Table S12 The first twenty singlet (S_n) excited states of **1'**–**4'** computed by TDDFT/CPCM (dichloromethane) at the optimized ground state geometries.

Complex	S_n	Excitation ^a (Coefficient) ^b	Vertical excitation wavelength / nm	f^c	
1'	S ₁	H→L (0.68)	576	3.024	
	S ₂	H→L+1 (0.69)	533	0.030	
	S ₃	H-1→L (0.68)	457	0.021	
	S ₄	H-1→L+1 (0.67)	443	0.702	
	S ₅	H→L+2 (0.66)	385	0.530	
	S ₆	H-2→L (0.66)	364	0.145	
	S ₇	H-2→L+1 (0.60)	359	0.026	
	S ₈	H→L+3 (0.63)	346	0.000	
	S ₉	H-1→L+2 (0.62)	331	0.000	
	S ₁₀		H-6→L (0.43)	325	0.019
			H-7→L+1 (0.35)		
			H-7→L (0.36)		
	S ₁₁		H-6→L+1 (0.36)	324	0.002
			H-4→L (0.33)		
			H-3→L (0.62)		
	S ₁₂		H-3→L (0.62)	321	0.002
	S ₁₃		H→L+4 (0.41)	320	0.011
	S ₁₄		H-4→L (0.47)	319	0.052
			H-7→L (0.30)		
	S ₁₅		H-5→L (0.43)	319	0.021
H-3→L+1 (-0.40)					
S ₁₆		H→L+4 (0.44)	311	0.203	
		H-4→L+1 (-0.36)			
		H-3→L+1 (0.30)			
S ₁₇		H-9→L (0.51)	307	0.030	
		H-8→L+1 (0.31)			
S ₁₈		H-9→L+1 (0.41)	306	0.011	
		H-8→L (0.37)			
		H-10→L (0.32)			
S ₁₉		H-3→L+1 (0.43)	305	0.007	
		H-5→L (0.43)			
S ₂₀		H-1→L+3 (0.66)	303	0.014	

2'	S ₁	H→L (0.68)	593	2.966
	S ₂	H→L+1 (0.69)	550	0.030
	S ₃	H-1→L (0.68)	468	0.024
	S ₄	H-1→L+1 (0.66)	455	0.756
	S ₅	H→L+2 (0.66)	399	0.543
	S ₆	H-2→L (0.46)	371	0.114
		H→L+3 (-0.39)		
	S ₇	H-2→L (0.48)	371	0.116
		H→L+3 (0.39)		
	S ₈	H-2→L+1 (0.55)	362	0.017
		H→L+3 (0.40)		
	S ₉	H-1→L+2 (0.64)	340	0.000
	S ₁₀	H→L+4 (0.53)	333	0.000
	S ₁₁	H-7→L (0.36)	330	0.009
		H-6→L+1 (0.34)		
		H-4→L (0.32)		
	S ₁₂	H-7→L+1 (0.35)	329	0.060
		H→L+4 (0.31)		
		H-6→L (0.31)		
	S ₁₃	H-3→L (0.62)	327	0.001
S ₁₄	H-4→L (0.43)	324	0.071	
S ₁₅	H-5→L (0.34)	324	0.063	
	H-3→L+1 (-0.31)			
S ₁₆	H-1→L+3 (0.39)	321	0.175	
	H-3→L+1 (0.33)			
S ₁₇	H-1→L+3 (0.51)	318	0.043	
	H-4→L+1 (0.35)			
S ₁₈	H-9→L (0.49)	312	0.026	
	H-8→L+1 (0.30)			
S ₁₉	H-3→L+1 (0.40)	311	0.013	
	H-9→L+1 (-0.32)			
S ₂₀	H-5→L (0.37)	310	0.000	
	H-10→L (0.30)			
3'	S ₁	H→L (0.69)	630	2.968
	S ₂	H→L+1 (0.70)	543	0.000
	S ₃	H-1→L (0.69)	445	0.000

S ₄	H-1→L+1 (0.58) H→L+2 (0.34)	415	0.787
S ₅	H-2→L (0.68)	403	0.004
S ₆	H-3→L (0.68)	398	0.000
S ₇	H→L+2 (0.59) H-1→L+1 (-0.37)	396	0.011
S ₈	H-4→L (0.66)	385	0.122
S ₉	H-2→L+1 (0.48) H-5→L (-0.45)	373	0.000
S ₁₀	H-2→L+1 (0.49) H-5→L (0.44)	369	0.000
S ₁₁	H-3→L+1 (0.68)	366	0.001
S ₁₂	H→L+3 (0.62)	354	0.000
S ₁₃	H-4→L+1 (0.58)	352	0.000
S ₁₄	H-6→L (0.63)	347	0.157
S ₁₅	H-7→L (0.68)	343	0.001
S ₁₆	H-5→L+1 (0.47) H-8→L (0.41)	342	0.062
S ₁₇	H-8→L (0.50) H-5→L+1 (-0.45)	339	0.062
S ₁₈	H-9→L (0.50)	330	0.000
S ₁₉	H-10→L (0.68)	329	0.002
S ₂₀	H-9→L (0.46)	329	0.000
4'			
S ₁	H→L (0.69)	646	2.978
S ₂	H→L+1 (0.70)	561	0.000
S ₃	H-1→L (0.69)	453	0.000
S ₄	H-1→L+1 (0.51) H→L+2 (-0.44)	428	0.828
S ₅	H-2→L (0.64)	412	0.009
S ₆	H→L+2 (0.49) H-1→L+1 (0.44)	409	0.030
S ₇	H-3→L (0.67)	407	0.000
S ₈	H-4→L (0.66)	393	0.135
S ₉	H-2→L+1 (0.58) H-5→L (-0.32)	382	0.000
S ₁₀	H-5→L (0.48)	377	0.000

	H-2→L+1 (0.35)		
S ₁₁	H-3→L+1 (0.67)	375	0.002
S ₁₂	H→L+3 (0.65)	375	0.000
S ₁₃	H-4→L+1 (0.62)	361	0.000
	H-5→L (-0.33)		
S ₁₄	H-6→L (0.57)	353	0.180
	H-5→L+1 (-0.32)		
S ₁₅	H-5→L+1 (0.53)	350	0.018
	H-6→L (0.38)		
S ₁₆	H-7→L (0.68)	349	0.000
S ₁₇	H-8→L (0.59)	346	0.160
S ₁₈	H-6→L+1 (0.35)	337	0.001
	H-8→L+1 (0.34)		
	H-1→L+2 (-0.33)		
S ₁₉	H-9→L (0.61)	335	0.000
S ₂₀	H-10→L (0.62)	335	0.002

^a The orbitals involved in the excitation (H = HOMO and L = LUMO).

^b The coefficients in the configuration interaction (CI) expansion that are less than 0.3 are not listed.

^c Oscillator strengths.

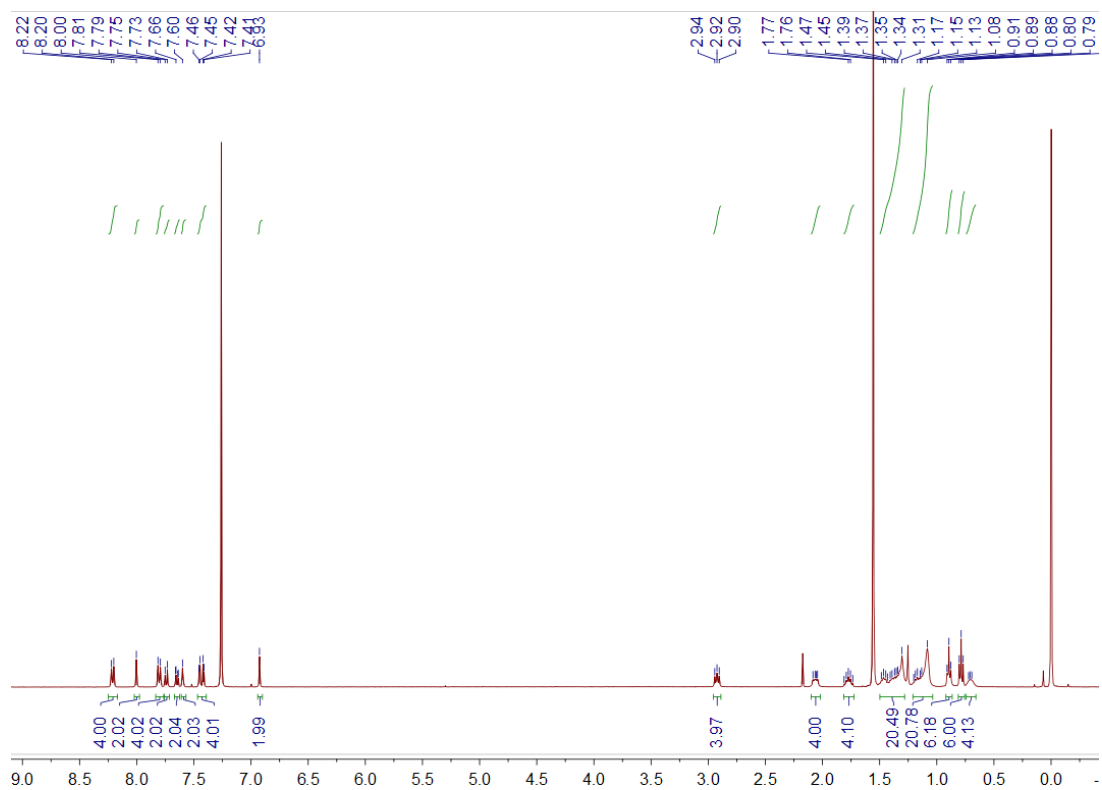


Fig. S27 ^1H NMR spectrum of **1** in CDCl_3 .

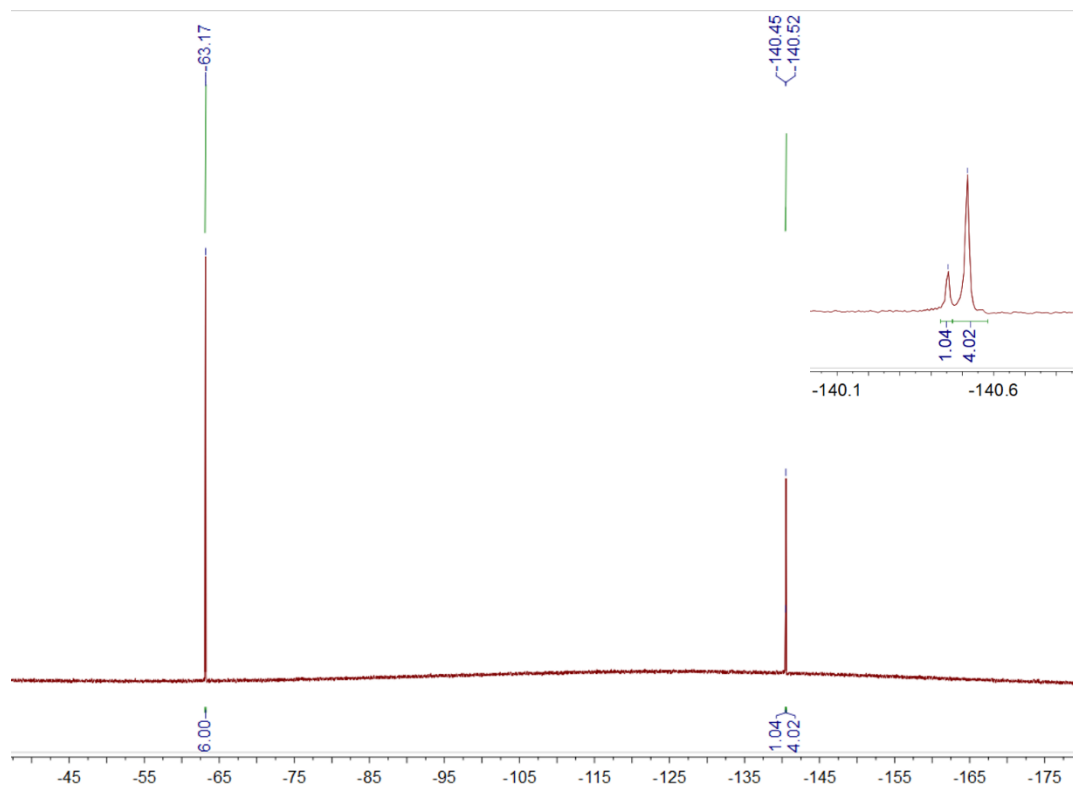


Fig. S28 $^{19}\text{F}\{^1\text{H}\}$ NMR spectrum of **1** in CDCl_3 .

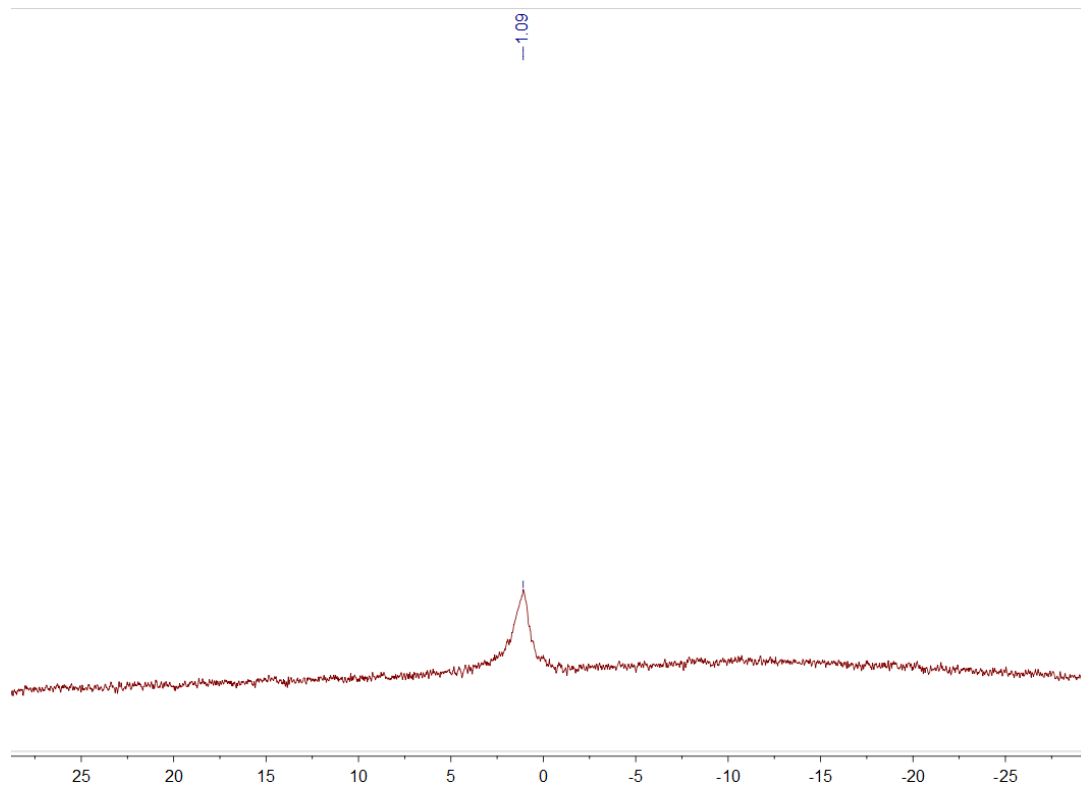


Fig. S29 $^{11}\text{B}\{^1\text{H}\}$ NMR spectrum of **1** in CDCl_3 .

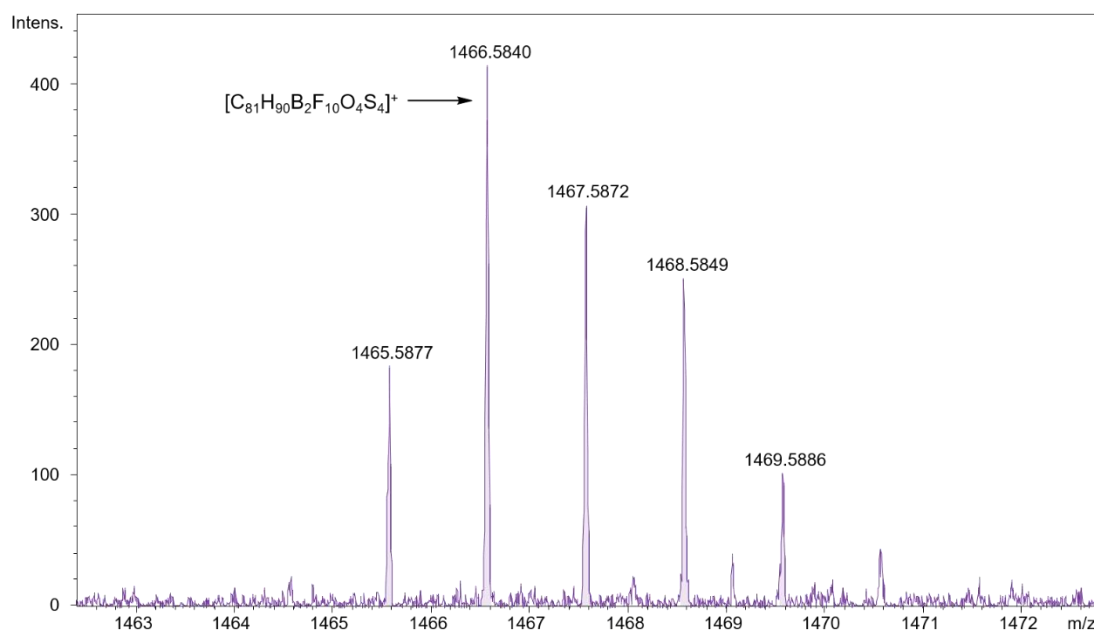


Fig. S30 HR-ESI mass spectrum of **1**.

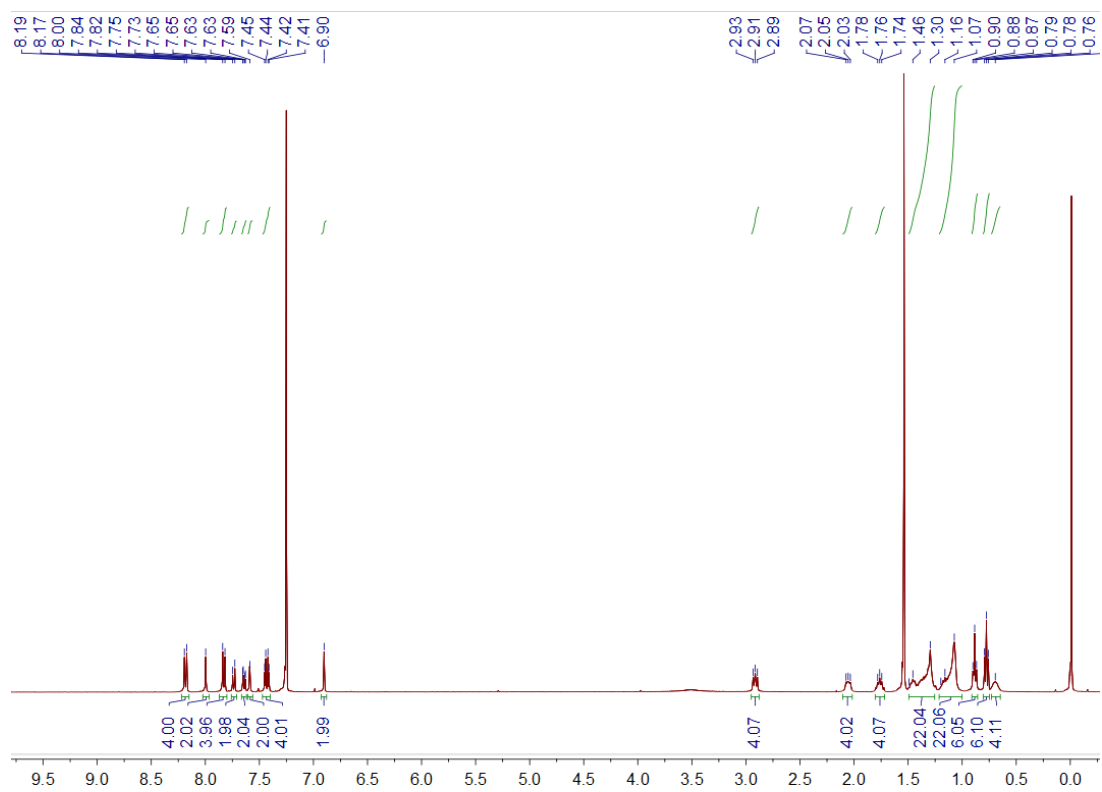


Fig. S31 ^1H NMR spectrum of **2** in CDCl_3 .

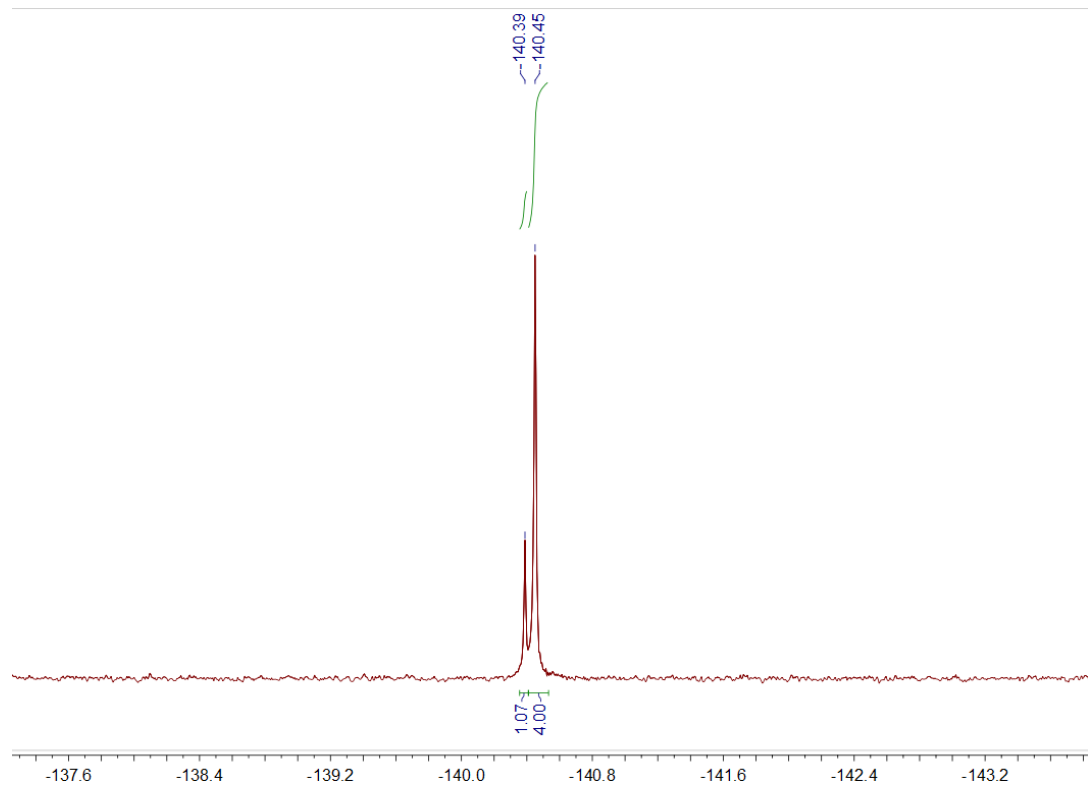


Fig. S32 $^{19}\text{F}\{^1\text{H}\}$ NMR spectrum of **2** in CDCl_3 .

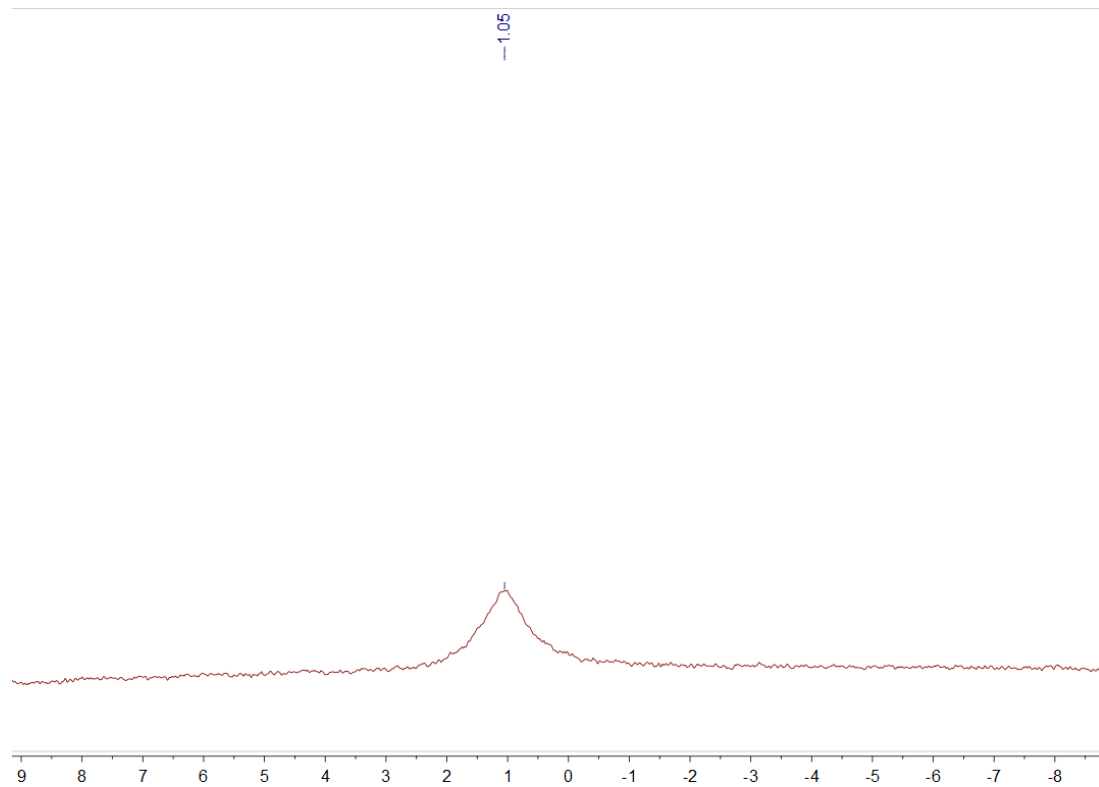


Fig. S33 $^{11}\text{B}\{^1\text{H}\}$ NMR spectrum of **2** in CDCl_3 .

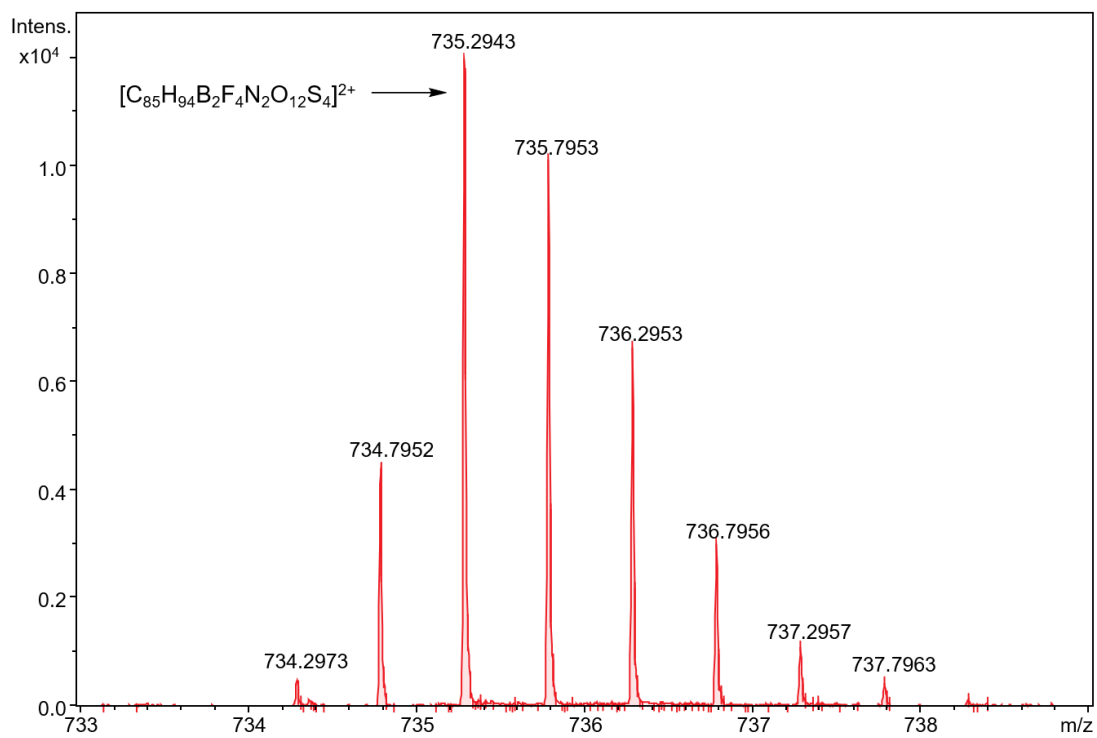


Fig. S34 HR-ESI mass spectrum of **2**.

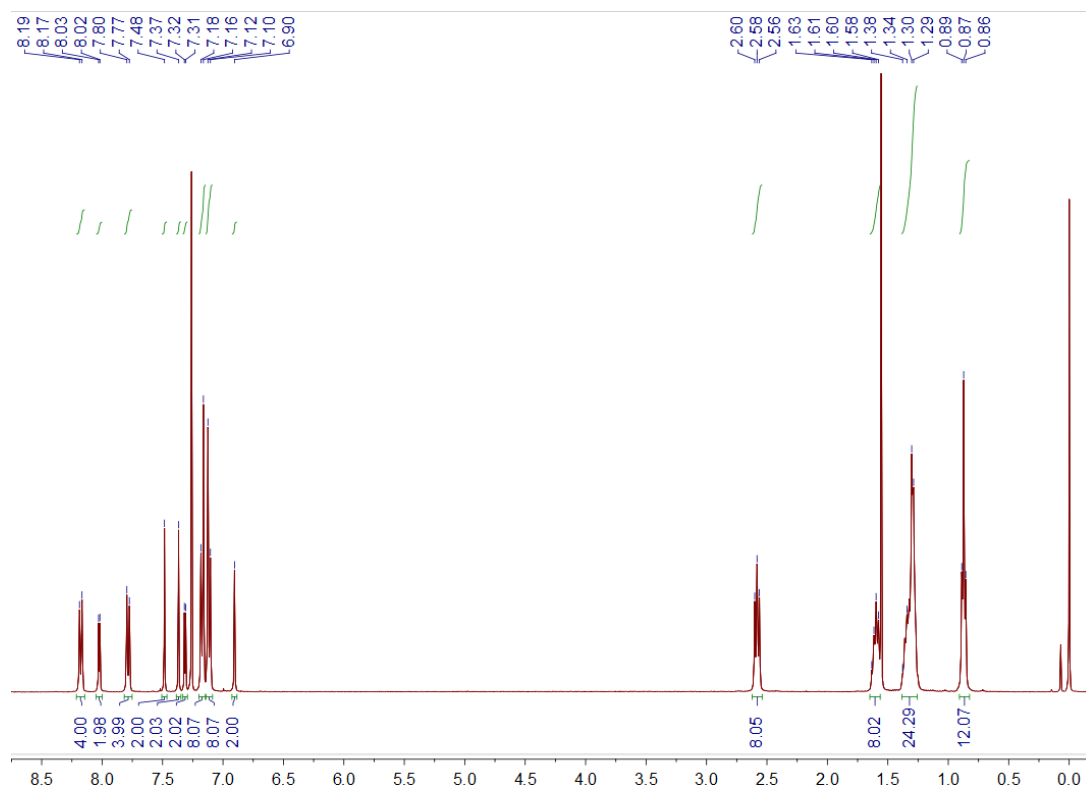


Fig. S35 ^1H NMR spectrum of **3** in CDCl_3 .

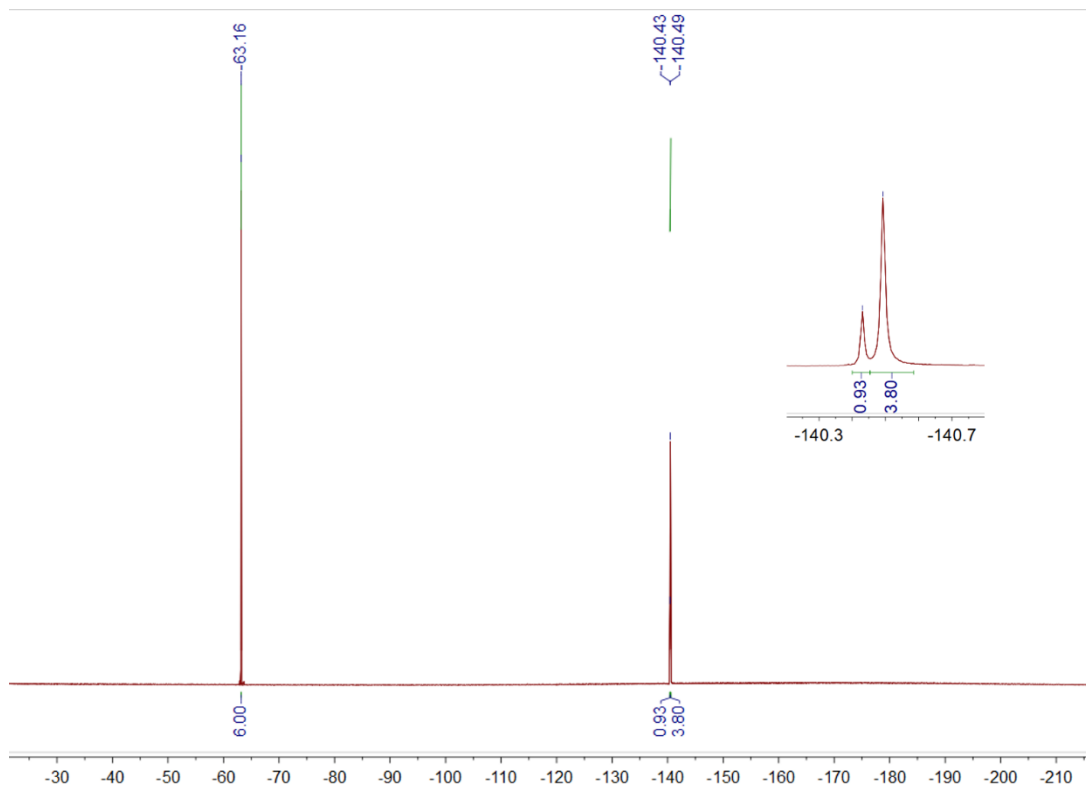


Fig. S36 $^{19}\text{F}\{^1\text{H}\}$ NMR spectrum of **3** in CDCl_3 .

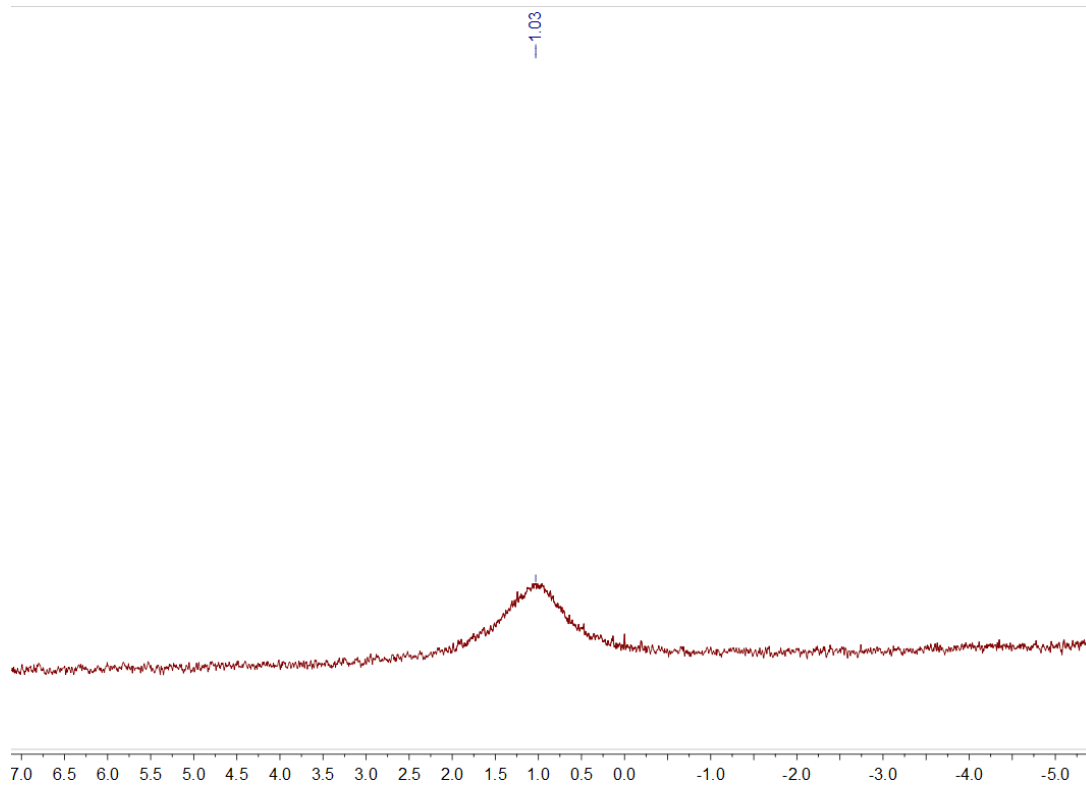


Fig. S37 $^{11}\text{B}\{^1\text{H}\}$ NMR spectrum of **3** in CDCl_3 .

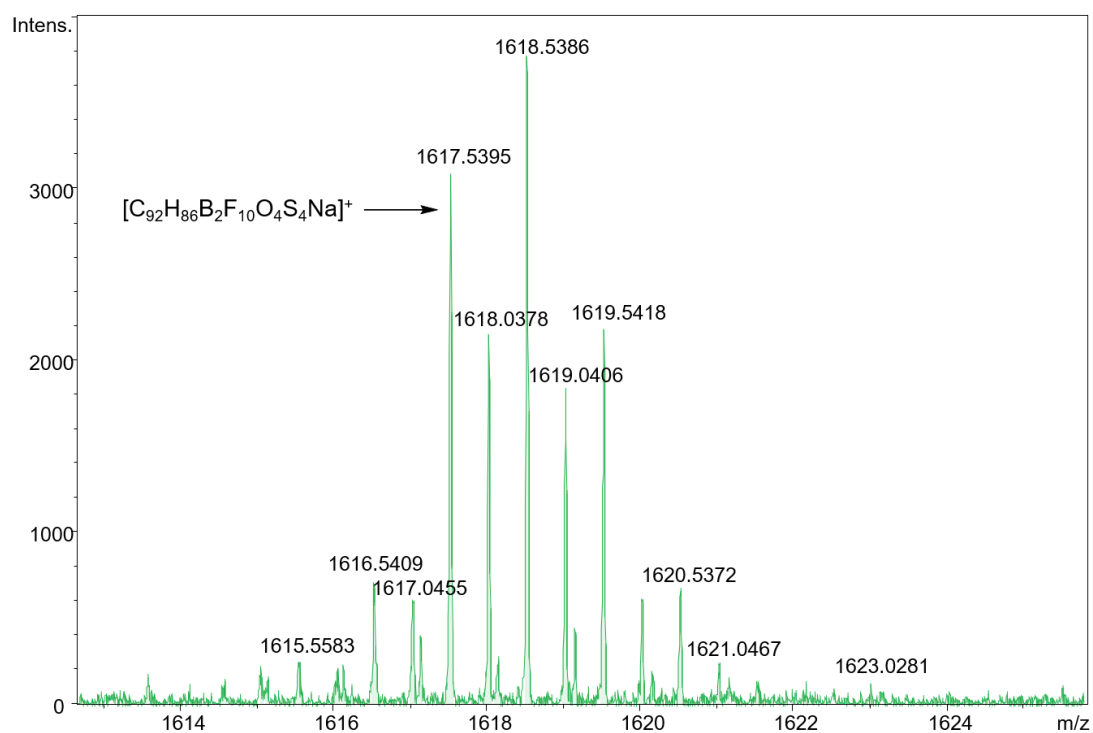


Fig. S38 HR-ESI mass spectrum of **3**.

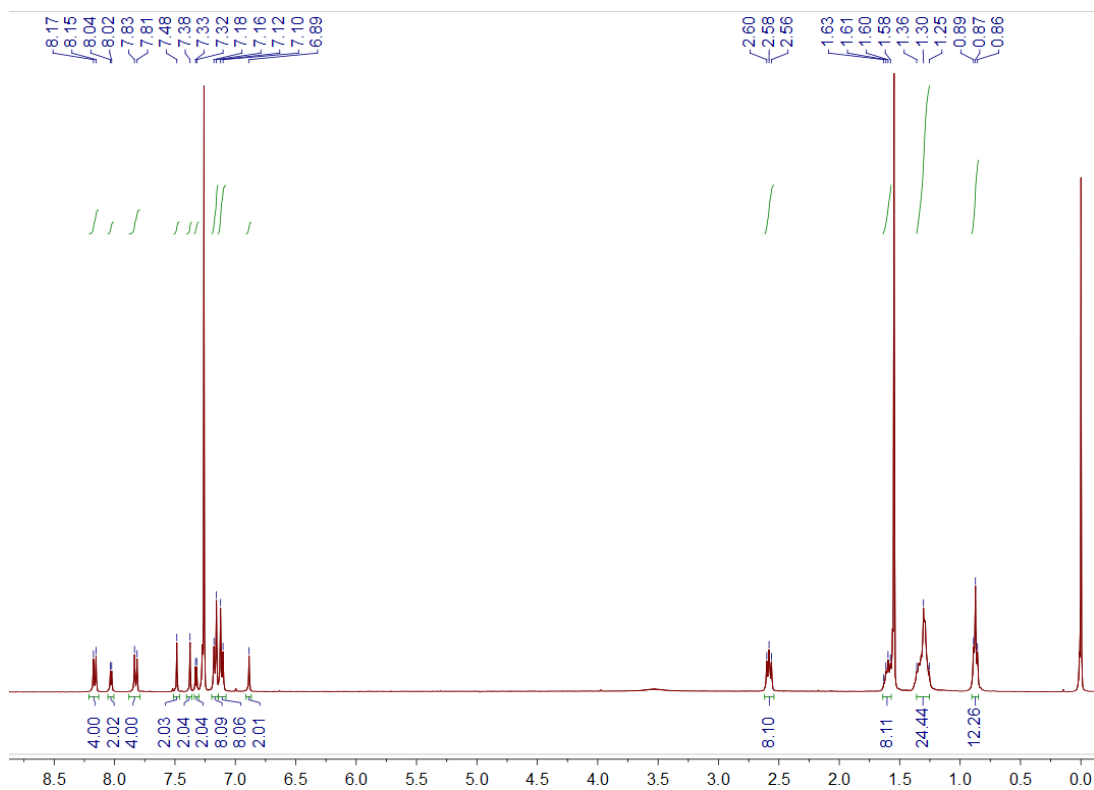


Fig. S39 ^1H NMR spectrum of **4** in CDCl_3 .

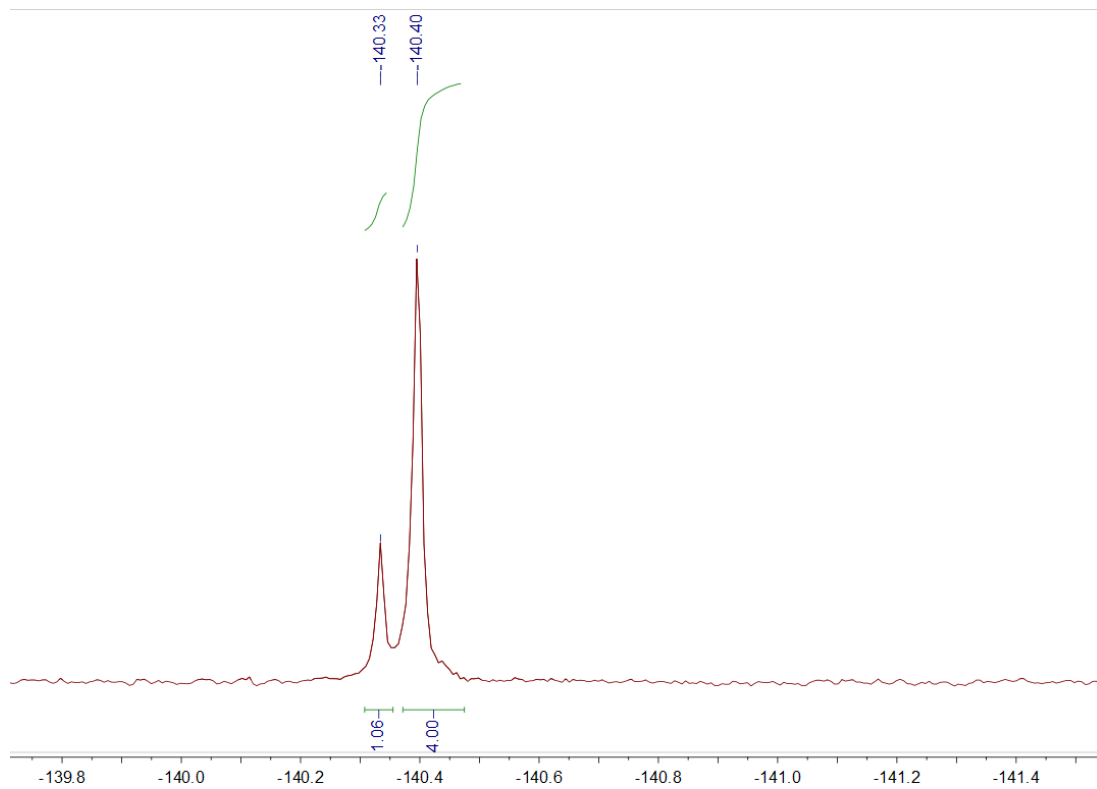


Fig. S40 $^{19}\text{F}\{^1\text{H}\}$ NMR spectrum of **4** in CDCl_3 .

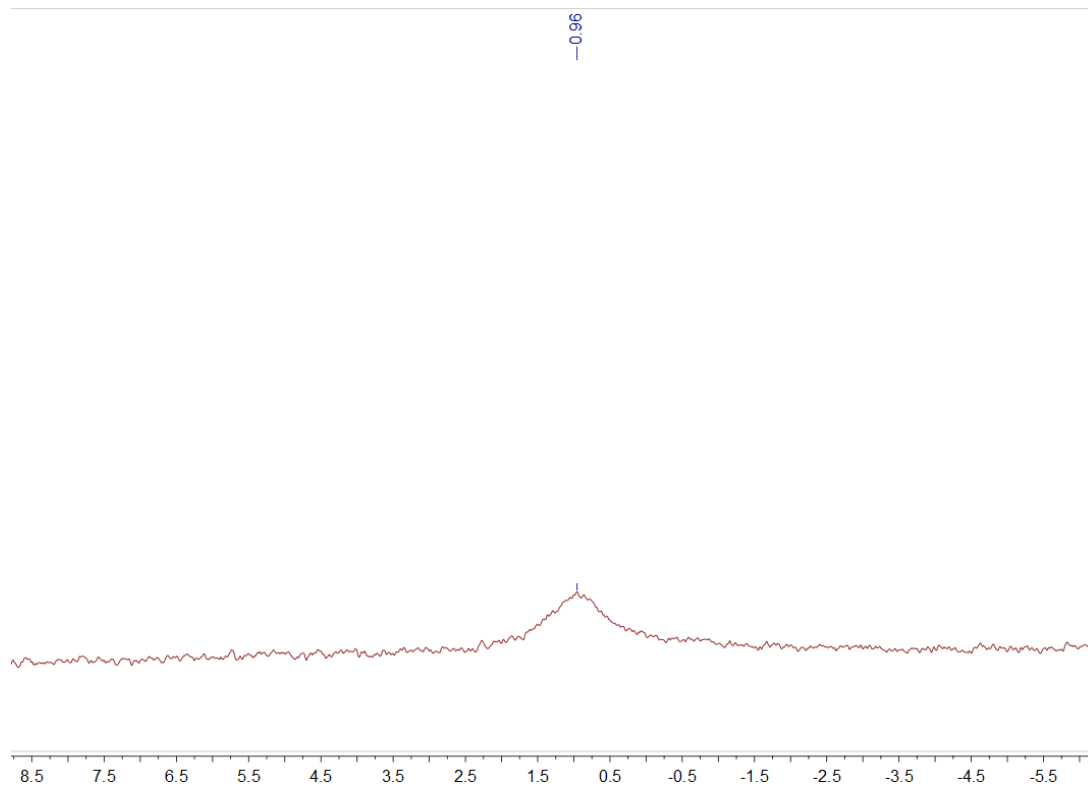


Fig. S41 $^{11}\text{B}\{^1\text{H}\}$ NMR spectrum of **4** in CDCl_3 .

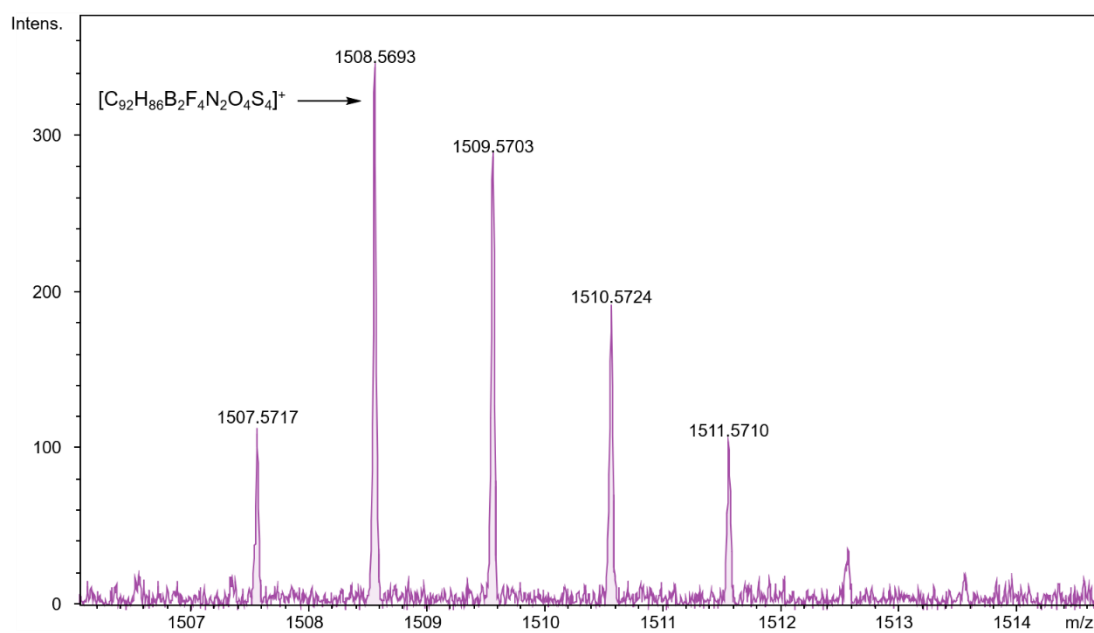


Fig. S42 HR-ESI mass spectrum of **4**.

References

- 1 J.-L. Wang, Q.-R. Yin, J.-S. Miao, Z. Wu, Z.-F. Chang, Y. Cao, R.-B. Zhang, J.-Y. Wang, H.-B. Wu, Y. Cao, *Adv. Funct. Mater.* **2015**, *25*, 3514–3523.
- 2 Y. Zhang, J. Zou, H.-L. Yip, K.-S. Chen, D. F. Zeigler, Y. Sun, A. K. Y. Jen, *Chem. Mater.* **2011**, *23*, 2289–2291.
- 3 Y. Lin, F. Zhao, Y. Wu, K. Chen, Y. Xia, G. Li, S. K. K. Prasad, J. Zhu, L. Huo, H. Bin, Z.-G. Zhang, X. Guo, M. Zhang, Y. Sun, F. Gao, Z. Wei, W. Ma, C. Wang, J. Hodgkiss, Z. Bo, O. Inganäs, Y. Li, X. Zhan, *Adv. Mater.* **2017**, *29*, 1604155.
- 4 V. K.-M. Au, D. Wu and V. W.-W. Yam, *J. Am. Chem. Soc.* **2015**, *137*, 4654–4657.
- 5 C.-T. Poon, D. Wu and V. W.-W. Yam, *Angew. Chem., Int. Ed.* **2016**, *55*, 3647–3651.
- 6 Y. Li, Z. Wang, C. Zhang, P. Gu, W. Chen, H. Li, J. Lu and Q. Zhang, *ACS Appl. Mater. Interfaces* **2018**, *10*, 15971–15979.
- 7 B. K. Barman, M. M. Guru, G. K. Panda, B. Maji and R. K. Vijayaraghavan, *Chem. Commun.* **2019**, *55*, 4643–4646.
- 8 X. Cheng, A. Md, H. Lian, Z. Zhong, H. Guo, Q. Dong and V. A. L. Roy, *J. Organomet. Chem.* **2019**, *892*, 34–40.
- 9 Y.-H. Cheng, H.-L. Wong, E. Y.-H. Hong, S.-L. Lai, M.-Y. Chan and V. W.-W. Yam, *ACS Appl. Energy Mater.* **2020**, *3*, 3059–3070.
- 10 C.-L. Wong, M. Ng, E. Y.-H. Hong, Y.-C. Wong, M.-Y. Chan and V. W.-W. Yam, *J. Am. Chem. Soc.*, 2020, *142*, 12193–12206.
- 11 M. J. Frisch, G. W. Trucks, H. B. Schlegel, G. E. Scuseria, M. A. Robb, J. R. Cheeseman, G. Scalmani, V. Barone, B. Mennucci, G. A. Petersson, H. Nakatsuji, M. Caricato, X. Li, H. P. Hratchian, A. F. Izmaylov, J. Bloino, G. Zheng, J. L. Sonnenberg, M. Hada, M. Ehara, K. Toyota, R. Fukuda, J. Hasegawa, M. Ishida, T. Nakajima, Y. Honda, O. Kitao, H. Nakai, T. Vreven, Jr., J. A. Montgomery, J. E. Peralta, F. Ogliaro, M. Bearpark, J. J. Heyd, E. Brothers, K. N. Kudin, V. N. Staroverov, T. Keith, R. Kobayashi, J. Normand, K. Raghavachari, A. Rendell, J. C. Burant, S. S. Iyengar, J. Tomasi, M. Cossi, N. Rega, J. M. Millam, M. Klene, J.

- E. Knox, J. B. Cross, V. Bakken, C. Adamo, J. Jaramillo, R. Gomperts, R. E. Stratmann, O. Yazyev, A. J. Austin, R. Cammi, C. Pomelli, J. W. Ochterski, R. L. Martin, K. Morokuma, V. G. Zakrzewski, G. A. Voth, P. Salvador, J. J. Dannenberg, S. Dapprich, A. D. Daniels, O. Farkas, J. B. Foresman, J. V. Ortiz, J. Cioslowski, D. J. Fox, (Gaussian 09, Revision D.01), Gaussian, Inc.: Wallingford, CT, 2013.
- 12 J. P. Perdew, K. Burke, M. Ernzerhof, *Phys. Rev. Lett.* **1996**, *77*, 3865–3868.
- 13 J. P. Perdew, K. Burke, M. Ernzerhof, [Phys. Rev. Lett. 77, 3865 (1996)]. *Phys. Rev. Lett.* **1997**, *78*, 1396–1396.
- 14 C. Adamo, V. Barone, *J. Chem. Phys.* **1999**, *110*, 6158–6170.
- 15 M. Cossi, N. Rega, G. Scalmani, V. Barone, *J. Comput. Chem.* **2003**, *24*, 669–681.
- 16 V. Barone, M. Cossi, *J. Phys. Chem. A* **1998**, *102*, 1995–2001.
- 17 R. Bauernschmitt, R. Ahlrichs, *Chem. Phys. Lett.* **1996**, *256*, 454–464.
- 18 M. E. Casida, C. Jamorski, K. C. Casida, D. R. Salahub, *J. Chem. Phys.* **1998**, *108*, 4439–4449.
- 19 R. E. Stratmann, G. E. Scuseria, M. J. Frisch, *J. Chem. Phys.* **1998**, *109*, 8218–8224.
- 20 W. J. Hehre, R. Ditchfield, J. A. Pople, *J. Chem. Phys.* **1972**, *56*, 2257–2261.
- 21 P. C. Hariharan, J. A. Pople, *Theor. Chim. Acta* **1973**, *28*, 213–222.
- 22 M. M. Francl, W. J. Pietro, W. J. Hehre, J. S. Binkley, M. S. Gordon, D. J. DeFrees, J. A. Pople, *J. Chem. Phys.* **1982**, *77*, 3654–3665.